



HAL
open science

Offshore Geological Hazards: Charting the Course of Progress and Future Directions

Gemma Ercilla, David Casas, Belén Alonso, Daniele Casalbore, Jesús Galindo-Zaldívar, Soledad García-Gil, Eleonora Martorelli, Juan-Tomás Vázquez, María Azpiroz-Zabala, Damien Do Couto, et al.

► **To cite this version:**

Gemma Ercilla, David Casas, Belén Alonso, Daniele Casalbore, Jesús Galindo-Zaldívar, et al.. Offshore Geological Hazards: Charting the Course of Progress and Future Directions. *Oceans*, 2021, 2 (2), pp.393 - 428. 10.3390/oceans2020023 . hal-03251755

HAL Id: hal-03251755

<https://hal.sorbonne-universite.fr/hal-03251755v1>




















Submitted on 7 Jun 2021

HAL is a multi-disciplinary open access archive for the deposit and dissemination of scientific research documents, whether they are published or not. The documents may come from teaching and research institutions in France or abroad, or from public or private research centers.

L'archive ouverte pluridisciplinaire **HAL**, est destinée au dépôt et à la diffusion de documents scientifiques de niveau recherche, publiés ou non, émanant des établissements d'enseignement et de recherche français ou étrangers, des laboratoires publics ou privés.

Review

Offshore Geological Hazards: Charting the Course of Progress and Future Directions

Gemma Ercilla ^{1,*}, David Casas ¹, Belén Alonso ¹ , Daniele Casalbore ² , Jesús Galindo-Zaldívar ³ , Soledad García-Gil ⁴, Eleonora Martorelli ⁵, Juan-Tomás Vázquez ⁶ , María Azpiroz-Zabala ⁷ , Damien DoCouto ⁸ , Ferran Estrada ¹ , M^a Carmen Fernández-Puga ⁹ , Lourdes González-Castillo ³, José Manuel González-Vida ¹⁰ , Javier Idárraga-García ¹¹ , Carmen Juan ¹² , Jorge Macías ¹³ , Asier Madarieta-Txurruka ³ , José Nespereira ¹⁴ , Desiree Palomino ⁶ , Olga Sánchez-Guillamón ⁶ , Víctor Tendoro-Salmerón ³ , Manuel Teixeira ^{15,16,17}, Javier Valencia ¹⁸  and Mariano Yenes ¹⁴ 

- ¹ Continental Margins Group, Consejo Superior de Investigaciones Científicas (CSIC), Instituto de Ciencias del Mar, Paseo Marítimo de la Barceloneta 37–49, 08003 Barcelona, Spain; davidcasas@icm.csic.es (D.C.); belen@icm.csic.es (B.A.); festrada@icm.csic.es (F.E.)
- ² Dipartimento di Scienze della Terra, Università di Roma “Sapienza”, Piazzale Aldo Moro 5, 00185 Rome, Italy; daniele.casalbore@uniroma1.it
- ³ Departamento de Geodinámica, Instituto Andaluz de Ciencias de la Tierra (IACT)–CSIC, Universidad de Granada, 18071 Granada, Spain; jgalindo@ugr.es (J.G.-Z.); lgcastillo@ugr.es (L.G.-C.); amadatxu@ugr.es (A.M.-T.); vtendoro@ugr.es (V.T.-S.)
- ⁴ BASAN, Centro de Investigación Mariña, Departamento de Geociencias Marinas, Universidade de Vigo, 36200 Vigo, Spain; sgit@uvigo.es
- ⁵ Istituto di Geologia Ambientale e Geoingegneria, Sede Secondaria di Roma, Consiglio Nazionale delle Ricerche (CNR), Piazzale A. Moro, 5, 00185 Rome, Italy; eleonora.martorelli@cnr.it
- ⁶ Instituto Español de Oceanografía—IEO, 29640 Malaga, Spain; juantomas.vazquez@ieo.es (J.-T.V.); desiree.palomino@ieo.es (D.P.); olga.sanchez@ieo.es (O.S.-G.)
- ⁷ Applied Geology, Civil Engineering and Geosciences, Delft University of Technology, Stevinweg 1, 2628 Delft, The Netherlands; emezeta@gmail.com
- ⁸ UMR 7193, Institut des Sciences de la Terre Paris (ISTeP), CNRS, Sorbonne Université, F-75005 Paris, France; damien.do_couto@sorbonne-universite.fr
- ⁹ Departamento de Ciencias de la Tierra, Facultad de Ciencias del Mar y Ambientales, INMAR (Instituto Universitario de Investigación Marina), Universidad de Cádiz, 11510 Cadiz, Spain; mcarmen.fernandez@uca.es
- ¹⁰ Departamento de Matemática Aplicada, Universidad de Málaga, Escuela de Ingenierías Industriales, Campus de Teatinos, s/n, 29071 Malaga, Spain; jgv@uma.es
- ¹¹ Departamento de Física y Geociencias, Universidad del Norte, 081007 Barranquilla, Colombia; idarragaj@uninorte.edu.co
- ¹² Laboratoire d’Oceanologie et de Géosciences, UMR, Université de Lille, CNRS, Université Littoral Côte d’Opale, F-59000 Lille, France; carmen.juanval@gmail.com
- ¹³ Departamento de Matemática Aplicada, Facultad de Ciencias, Universidad de Málaga, Campus de Teatinos, s/n, 29080 Malaga, Spain; jmacias@uma.es
- ¹⁴ Departamento de Geología, Universidad de Salamanca, 37008 Salamanca, Spain; jnj@usal.es (J.N.); myo@usal.es (M.Y.)
- ¹⁵ IDL (Laboratório Associado)—Instituto Dom Luíz, Campo Grande, Faculdade de Ciências da Universidade de Lisboa, Edifício C1, 1749-016 Lisboa, Portugal; mane.teixeira@gmail.com
- ¹⁶ Departamento de Geologia, Campo Grande, Faculdade de Ciências da Universidade de Lisboa, Edifício C6, 1749-016 Lisboa, Portugal
- ¹⁷ Divisão de Geologia Marinha e Georecursos Marinhos, IPMA—Instituto Português do Mar e da Atmosfera, Rua C do Aeroporto, 1749-077 Lisboa, Portugal
- ¹⁸ LYRA, Engineering Consulting, 01015 Gazteiz, Spain; javi.valencia.m@gmail.com
- * Correspondence: gemma@icm.csic.es



Citation: Ercilla, G.; Casas, D.; Alonso, B.; Casalbore, D.; Galindo-Zaldívar, J.; García-Gil, S.; Martorelli, E.; Vázquez, J.-T.; Azpiroz-Zabala, M.; DoCouto, D.; et al. Offshore Geological Hazards: Charting the Course of Progress and Future Directions. *Oceans* **2021**, *2*, 393–428. <https://doi.org/10.3390/oceans2020023>

Academic Editor: Pere Masqué

Received: 16 December 2020

Accepted: 24 May 2021

Published: 31 May 2021

Publisher’s Note: MDPI stays neutral with regard to jurisdictional claims in published maps and institutional affiliations.



Copyright: © 2021 by the authors. Licensee MDPI, Basel, Switzerland. This article is an open access article distributed under the terms and conditions of the Creative Commons Attribution (CC BY) license (<https://creativecommons.org/licenses/by/4.0/>).

Abstract: Offshore geological hazards can occur in any marine domain or environment and represent a serious threat to society, the economy, and the environment. Seismicity, slope sedimentary instabilities, submarine volcanism, fluid flow processes, and bottom currents are considered here because they are the most common hazardous processes; tsunamis are also examined because they are a secondary hazard generated mostly by earthquakes, slope instabilities, or volcanic eruptions. The hazards can co-occur and interact, inducing a cascading sequence of events, especially in certain

contexts, such as tectonic indentations, volcanic islands, and canyon heads close to the coast. We analyze the key characteristics and main shortcomings of offshore geological hazards to identify their present and future directions for marine geoscience investigations of their identification and characterization. This review establishes that future research will rely on studies including a high level of multidisciplinary. This approach, which also involves scientific and technological challenges, will require effective integration and interplay between multiscale analysis, mapping, direct deep-sea observations and testing, modelling, and linking offshore observations with onshore observations.

Keywords: seismic faults; slope instabilities; submarine volcanism; fluid-flow processes; bottom currents; tsunamis; canyon heads; tectonic indentation; multidisciplinary approach

1. Introduction

Geological processes occurring within or at the surface of the Earth may lead to natural disasters causing loss of life, environmental damage, and major impacts on the economy and food security. Human behavior may also trigger natural disaster processes where no hazards existed before or increase the risks where they do exist. Knowledge of the geological elements likely to produce a disaster and their distribution, as well as the understanding of the mechanisms (conditioning factors and triggers), is critical for the prevention and mitigation of catastrophic events [1–4]. The time scales of those mechanisms are highly variable, from geologic to human scale, which contrasts greatly with the sudden impact of such events when they are triggered.

Like in any other Earth domain, the marine environment is associated with potentially hazardous geological processes that may represent serious threats to society, the economy, and the environment (http://www.esf.org/fileadmin/Public_documents/Publications/Natural_Hazards.pdf, accessed on 28 May 2020) (Figure 1). Such processes are present in all physiographic domains; even features and events that occur on the continental shelf and in deep-sea areas may have catastrophic effects on large areas in coastal environments [5]. Coastal areas are highly populated around the world and are the sites of most megacities [6]. A growing population, currently approximately 2.4 billion people, lives within 100 km of the coast (oceanconference.un.org, accessed on 28 May 2020). The expansion of urban coastal areas and coastal and offshore industries (e.g., communications, energy, and mineral extraction) has greatly increased the exposure and risk of large subaerial and submarine infrastructure. Contrary to the social perception, submarine areas host different and active features that present frequent geohazards.

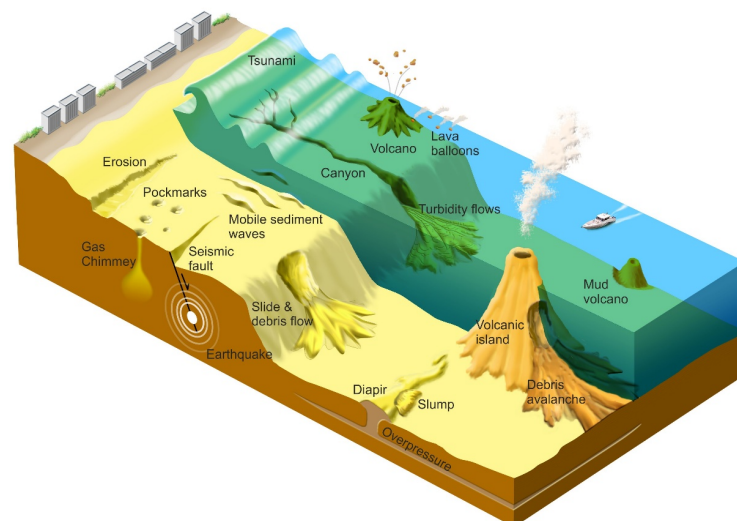


Figure 1. Sketch showing the main offshore geological hazards. Inspired by [7].

Avoidance of hazardous areas is not always possible. Therefore, to reduce the risk of an area, conceptualized as the product of hazards and vulnerability, it is imperative to reduce vulnerability and obtain better knowledge of hazardous processes through new approaches and the development of new techniques and tools [8,9].

The field of offshore geohazards is wide because it covers different topic areas, such as identification and mapping of the hazards, risks, vulnerability, predictions, and warnings; covering all of these topics is beyond the scope of this paper. Specifically, this paper aims to provide the summary of the course and progress in the research of geoscientists regarding the main offshore hazardous geological processes, namely: seismicity, slope sedimentary instabilities, submarine volcanism, fluid flow processes, bottom currents, and tsunamis. Some geological settings, where interactions arise from cascading effects and thus create multihazard scenarios, are also shown. We analyze the key characteristics and main shortcomings of those geohazards, enabling the identification of present and future directions for marine geosciences focusing on offshore geohazards.

2. Definition and Classification of Offshore Geological Hazards

There are several definitions of geological hazards (e.g., [10–12]). As a synthesis, geological hazards can be considered all phenomena or conditions (on land and offshore), natural or induced by human activity, that can produce damage and that geological information can be used to predict, prevent, or correct.

The classification of offshore geological hazards may vary depending on their implications. From an engineering point of view, they are generally classified based on the problems they can generate during the exploration, installation, and operation of structures [13]. In contrast, marine geoscientists are more interested in understanding the features and processes that define a hazard; therefore, they classify them according to their causes.

Offshore geohazards arise from different geomorphological and geological features that produce scenarios in which diverse processes may act alone or in combination with others, triggering a chain of events. Morphological characteristics, such as relief (negative or positive) or overstepped slopes, may be indicators of processes that can generate hazards; however, depending on the activity planned, they may be considered a threat themselves.

The most widespread offshore geohazards are seismicity, slope instabilities, submarine volcanism, and processes related to fluid flow and bottom currents (e.g., [5,7,9,14]; <https://niwa.co.nz/natural-hazards/marine-geological-hazards>; <https://marineboard.eu/marine-geohazards-blue-economy>, accessed on 3 October 2020) (Figure 1). Tsunamis deserve special mention because they are a secondary hazard derived from or generated by another event, especially earthquakes, slope instabilities, or volcanic eruptions ([5,15,16], among others). Additionally, many of these processes are associated with intense submarine erosion that may be responsible for the general topography and microtopography of the seafloor (e.g., [17]). Seismicity has a direct impact on the ground due to vibrations that affect infrastructure and buildings. Moreover, seismicity can also produce indirect effects, such as liquefaction and slope instabilities [18]. Earthquakes are related to the presence of seismogenic faults.

Submarine slope instabilities, resulting in products collectively referred to as landslides, mass-transport deposits, or mass-transport complexes, are capable of damaging infrastructure resting on or fixed to the seafloor, such as vertical foundations, communication cables, and pipelines, due to the associated impact, dragging, excessive burial, or undermining effects [19,20]. Active submarine volcanoes are significant geological hazards because of their violent and explosive eruptions and related earthquakes, collapses of their summits (i.e., caldera) and fluid emissions; moreover, volcanic activity can trigger secondary hazards such as tsunamis and landslides [5].

Fluid flow processes, such as seepage of light hydrocarbons, migration of overpressurized muddy fluids forming volcanoes and diapirs (Figure 1), and gas hydrate formation and breakdown, constitute a main type of potential geohazard [7,21]. They

are commonly a threat to navigation and offshore infrastructure, during both installation and operation, because they can cause damage or uncontrolled release of gas that in turn induces explosions or landslides.

The persistent action of bottom currents over the seafloor may create large areas affected by erosion and scouring and highly active seafloor conditions (Figure 1). Similarly, reworked or transported marine sediment is subsequently deposited, forming mounds in areas with high sedimentation rates. Bottom currents may also affect the sedimentological and geotechnical properties of seafloor and subsurface sediments, affecting their stability [22]. Thus, bottom currents may represent a hazardous process to subsurface and seafloor installations and infrastructure crossing the water column, because surface and intermediate currents can induce stress on them.

Human Activities in Submarine Environments

Human activities on the seafloor have increased sharply since the last half of the last century, accompanied by significant technological advances (Figure 2). Therefore, the understanding of offshore geological hazardous processes is fundamental for seafloor management. The main important offshore activities potentially exposed to offshore geohazards are as follows:

- a. Submarine telecommunication cables are important offshore infrastructure and funnel 95% of all telephone and data communication. Approximately 378 subsea cables (total length of 1.2 million kilometers) (<https://www.mapfreglobalrisks.com>, accessed on 12 October 2020) rest on the seafloor, forming complex inter-continental, inter-peninsular, and island-continent networks (<https://www.submarinecablemap.com/>, accessed on 3 February 2020). Some new deployments are designed to bury cables in the seafloor to protect them from trawlers, anchors, and turbidity currents [23].
- b. Ports and industrial installations, airports, residential and recreation buildings, artificial islands, wind farms, and fish farming, among others, are human-made structures occupying subaerial and submarine surfaces, and they will increase due to human expansion. These structures may be affected by geological processes, but they may also be affected by potential human-induced hazards because of the interaction between seafloor structures and environmental processes.
- c. Deep-sea mining has the potential to be an important submarine activity in the near future. This activity involves prospecting, exploitation, and extraction [24], and all three stages are subject to hazardous geological processes.
- d. Fisheries and transport are critical economic activities around the world. Fishing grounds and commercial routes (navigation) may be locally affected by active geological processes occurring on the seafloor.
- e. Hydrocarbon exploitation and transportation are performed by 53 countries on continental shelves and adjacent slopes, where the deployed infrastructure is placed on the seabed and interacts with geological processes during installation and operation [13].
- f. Gas and oil pipelines, in contrast to the exploitation platforms whose activities focus on the local seabed, cross different physiographic regions on the continental margins and are therefore affected by different hazardous geological processes, which may deform and rupture them. In 2016, operators planned nearly 4000 miles of offshore pipelines through 2020 (<https://www.offshore-mag.com/pipelines/article/16754997/>, accessed on 28 October 2020).
- g. Other common activities, such as sand recovery for the artificial nourishment of beaches, may represent hazards themselves because they may modify the sedimentary environment and natural processes.

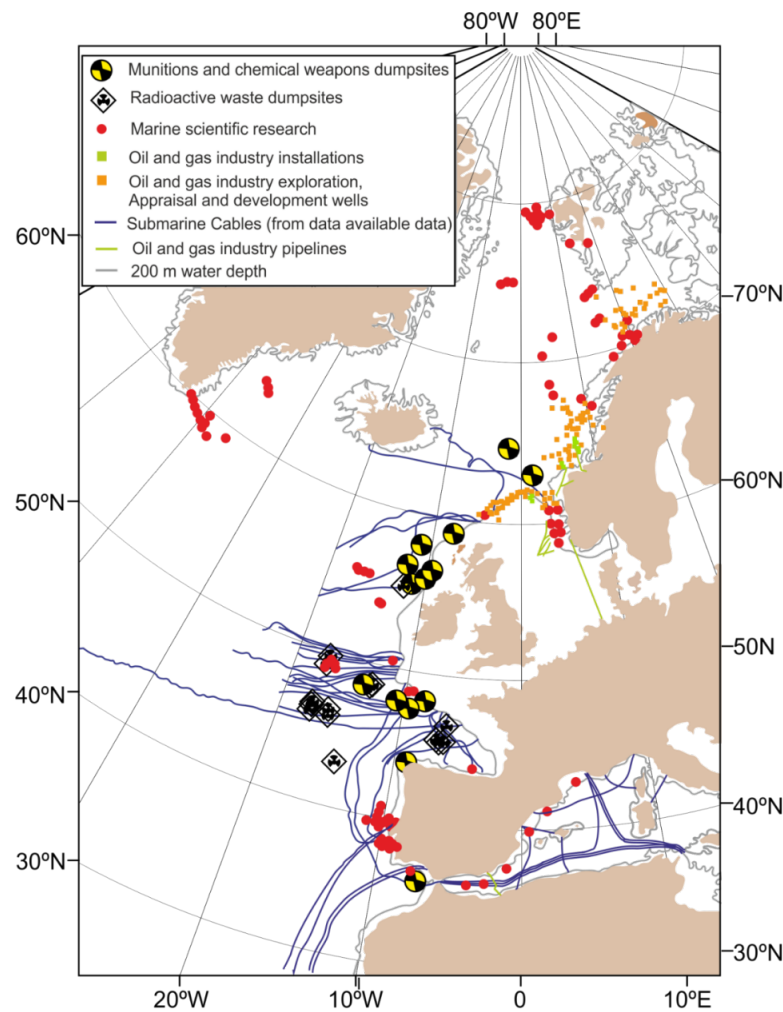


Figure 2. Some of the main human activities in deep-sea areas (>200 m water depth) in the NE Atlantic and western Mediterranean. The figure was used as idea and base to create a new one including more information from [25].

3. Some Prehistorical and Historical Cases of Offshore Geohazard Events

Offshore geological hazard events are recognized in all cultures and in all seas and oceans but are most common on highly active continental margins associated with tectonic plate boundaries (<https://www.emdat.be/>, accessed on 28 October 2020). Table 1 presents a small percentage of them, with only some of the widely known case events. All these disasters generated by prehistoric and historic marine geological events affected coastal populations, infrastructure, and the environment, highlighting the great vulnerability of these areas as well as the scarce knowledge regarding the triggering mechanisms of the events in particular or of the hazards in general. They have also revealed that active geological features do not recognize political frontiers and that hazard assessment must cross national boundaries. Furthermore, their occurrences have revealed that even small events may have a large impact on intensively exploited coasts (e.g., industry or tourism).

Table 1. Some prehistorical and historical cases of marine geohazard events.

Offshore Geohazard	Prehistorical and Historical Cases	Consequences
Earthquakes related to seismogenic faults	The 2011 Japan earthquake (North Pacific Ocean) of magnitude 9 (Mw) [26].	It caused an up to 30-m-high tsunami that flooded 110 km of coastline. Nearly 16,000 people were killed, and more than 400,000 buildings collapsed.
	The 2010 Chile earthquake (South Pacific Ocean) magnitude of 8.8 Mw [27].	It caused a tsunami with wave heights up to 30 m in the Chilean coastal region. It is the largest event along the South American Subduction Zone in half a century and produced 648 casualties.
	The 2004 Indian earthquake (Indian Ocean) of magnitude of 9.3 Mw [28].	It caused an up to 34 m-high-tsunami that produced an estimated 228 k casualties. This is one of the ten worst earthquakes in recorded history.
	The Al-Hoceima earthquake (SW Mediterranean) 1993–1994, 2004, and 2016 seismic crisis [29].	This event killed 464 people and caused 11.9 million Euros of economic losses in Spain.
	The 1908 Messina earthquake (NW Mediterranean) of magnitude 7.1 (Mw) with the epicenter in the Messina Strait graben [30].	It produced a local tsunami. It is the most destructive 20th and 21st century earthquake in Europe, with >80,000 deaths.
Slope instabilities	The 1906 San Francisco earthquake (North Pacific Ocean) of magnitude 8.3 (Mw) with the epicenter located on the San Andreas Fault [31].	The economic impact was tremendous. The impact is assessed as US \$524 million, and the earthquake left more than 3000 people dead and more than 28,000 buildings destroyed.
	The 1979 Lomblen landslide (between the Indian Ocean and the Pacific Ocean) that generated a strong tsunami with heights of 7–9 m [32].	It caused 539 casualties and another 700-missing people.
	The 1979 Nice submarine landslide (NW Mediterranean) related to the construction of the new Nice harbor [33].	It generated a tsunami (wave heights to 3 m) and is probably one of the most important geological events to have occurred in France within the last 20 years. It caused casualties and considerable material damage [34].
	The 1929 Grand Banks slide (Northern Atlantic Ocean) was triggered by an earthquake (magnitude of 7.2 Ms) [35].	It generated a tsunami that killed 28 people and severed several submarine communication cables.
Volcanism eruptions and slope instabilities on volcano flanks	The Storegga Slide (Norwegian Sea), approximately 8200 years ago [36,37] off the Norwegian coast.	It generated a tsunami that hit the west coast of Norway (run up 10–12 m), Scotland (4–6 m), Shetland (approx. 20–30 m), and the Faroes (0–10 m) [38].
	The 1950 AD Santorini active volcanic eruptions (Aegean Sea) [39].	They produced debris flows on the flanks of Santorini Island that produced damage and casualties.
	On active Hawaiian volcanoes (Pacific Ocean), large, rapid flank movements often co-occur with large earthquakes. They were observed four times during the 19th and 20th centuries, each spaced approximately 50 years apart [40].	They affected the quality of life of local people living on the islands and impacted on the islands' economies.
	The 2011 Hierro submarine eruption [41].	It affected the quality of life of local people living on the island and impacted on the island's economy, which was based primarily on tourism.
	Active Azores volcanoes are affected by diffuse CO ₂ emissions related to hydrothermal activity [42].	They may represent a public health risk, and occasionally family houses were evacuated when CO ₂ concentrations in the air reached 8 mol%

Table 1. Cont.

Offshore Geohazard	Prehistorical and Historical Cases	Consequences
Fluid flow (gas, mud, and salt diapirs)	Events associated with active pockmarks (up to 15 m deep) on the seafloor of the off Patras and Aigion (northern Peloponnese, Greece) [43].	These pockmarks were found to be venting gas prior to the earthquake (the M 5.4) on 14 July 1993.
	Catastrophic gas escape during the exploration drilling in the German Bight of the North Sea in 1963, the J. Storm II in 1972 [44] and in the North Sea in 1990.	Gas escape formed large, deep pockmarks over very short periods.
Erosion, scour, and seabed mobility by bottom currents	The Arklow Bank Wind Farm, the best wind resources in the Irish Sea was subjected to overall seabed movement [45].	Movement of the sandbank, channel migration, and overall erosion and accretion. Scouring was caused by the strong currents that flowed over the sandbank, often over 2 m/s.
	In the gravity-based foundations of the Frigg TP1 GBS, installed in fine sand soil at 104 m of water depth, in the North Sea [46,47].	2 m deep scour erosion at two corners.
	Several submarine pipeline failures in the Mississippi River delta and the Gulf of Mexico [48,49].	Seabed erosion by scouring around the pipe under the influence of currents caused the pipeline to be unsupported.

4. Offshore Geohazards and Their Main Key Questions

4.1. Tectonic Earthquakes: Seismogenic Faults

Internal geodynamic processes constitute the main engine that determines the present-day Earth's configuration. Most of the plate boundaries are located in offshore areas where seismically active faults constitute a principal marine threat [50,51]. In addition, some of them continue onshore, providing a good chance for direct observations (e.g., San Andreas Fault, [52]; the Alpine Fault, [53]). Progressive and continuous plate motion is accommodated by deformation along the plate boundaries where most of the active faults are located [54,55]. Some faults may undergo creep and are aseismic [56]. However, in sectors where two large fault blocks become coupled by asperities on the fault surface, elastic deformation, and stresses may increase, reaching the strength of the rocks [57]. The above factors drive sudden slip, producing an earthquake and, as a result, seafloor shaking, liquefaction, and permanent deformation [58].

Thrust faults related to subduction zones, including those associated with the Ring of Fire surrounding the Pacific Ocean and in the Indian Ocean, produce the most intense earthquakes [59–61] (Figure 3a). In these regions, although deep seismicity occurs, the most devastating earthquakes are located at shallow depths close to the coastlines. Examples include the Alaska (1964, Mw 9.2), Sumatra (2004, Mw 9.0–9.3.1), Chile (2010/1960, Mw 8.89.5), and Japan (2011, Mw 9) earthquakes and the related tsunamis [62] (<https://earthquake.usgs.gov/>, accessed on 11 September 2020). In addition, transcurrent faults can accumulate high stresses, eventually resulting in major strike-slip earthquakes, such as in Cape Mendocino in California (1992, Mw, 7.2) [63]. However, such pure strike-slip events generally do not produce vertical displacements of the seafloor in flat areas, although they may be significant when steep slopes are affected [64]. Regardless, seafloor deformation occurs in transpressional (e.g., Shackleton fracture zone, Figure 3b, [65,66]) and transtensional faults (e.g., Incrisis-Al Idrissi faults, Figure 3c, [29]). A particular setting occurs at the tips of such faults, where vertical displacement may trigger tsunamis [67]. Seismogenic normal faults are relatively scarce in marine environments and are most likely related to the isostatic response of the Earth's crust to ice loads close to coastal areas [68].

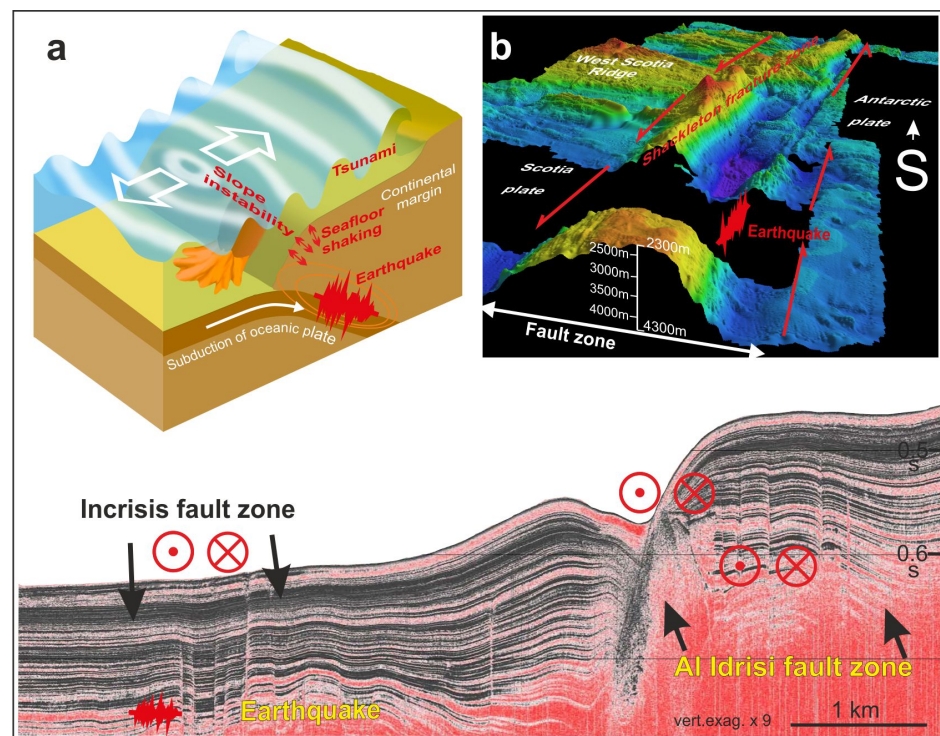


Figure 3. Examples of active seismogenic faults: (a) Subduction earthquakes in convergent plate margins have the highest magnitudes and produce seafloor shaking, submarine landslides, and tsunamis; (b) oblique-view perspective of the Shackleton fracture zone (Antarctica) that constitutes the transpressive sinistral active margin between the Scotia and Antarctic plates. Bathymetric features are determined by the permanent deformation of the seafloor; more details on this fracture zone can be found in [65,66]; (c) high-resolution seismic profile of the Incrisis and Al Idrisi sinistral fault zones in the central Alboran Sea, western Mediterranean. The tectonic activity of the Al Idrisi fault zone, now mostly covered by recent sediments, has been transferred to the new Incrisis fault zone, where the active faults affect the most recent sediments; more details on these fault zones in [29].

Detailed knowledge of fault features and their seismic characteristics is essential to preventing the effects of these geological hazards. The main target is to constrain the fault geometry, kinematics, dynamics, and seismic behavior to determine the related maximum magnitude of the seismic events and their recurrence interval. The numerical modelling of seafloor deformation and the propagation of seismic waves constitute one of the main tools to establish the direct impact of seismic waves on coastal populations and to determine the potential to produce submarine landslides and tsunamis. The determination of these key fault features and seismicity is developed either by coring, which allows the study of deposits related to the main events [69], or by geophysical methods. Seismological observations in areas surrounding active seismic zones are generally far from land, and the coverage of active seismic zones is limited, decreasing the accuracy of the locations of active seismogenic faults. Ocean bottom seismometers (OBSs) can record seismicity over long periods, but there are large delays in data recovery. Seismic reflection and acoustic techniques highlight the geometry of faults and improve the analysis of their activity. However, present-day standard techniques fail to produce a complete and detailed image of faults.

To improve the accurate analysis of the location and geometry of active faults, seafloor mapping of large parts of the oceans with new multibeam and sonar equipment is mandatory. The study of the continuity of faults at depth will require new seismic acquisition and data processing techniques, including 3D seismic methods for complex areas reaching depths of up to 12 km for crustal faults. The accuracy of seismological observations will increase with the installation of seafloor seismological observatories in wired networks to

provide real-time data. In addition, a denser network of OBSs will be necessary to achieve good coverage in active regions [50]. The characterization of fault behavior over long periods is also highlighted as new insight. In this sense, the improvement of submarine geomorphological indexes will likewise contribute to better identification and analysis of the active faults. Shallow coring techniques and detailed high-resolution seismic parametric profiles will improve the analysis of the geometry and age of the related deposits. These observations will help to determine the fault slip and the recurrence periods of the main submarine palaeoearthquake records. Deep coring techniques may enhance the significance of fluids in fault activity. In addition, the study of marine faults with offshore to onshore continuity will be essential for collecting direct observations of fault zones (fault surfaces, fault striations, fault gouges, and related deposits) and for determining their kinematics. Geodetic networks (global positioning system (GPS) and high-precision levelling (HPL)) and satellite-based Earth observations will also be mandatory to measure their present-day activity and constrain isostatic rebound in glacial margins close to the coastlines.

The integration of these new data will improve the probabilistic seismic hazard models in offshore tectonically active areas and the evaluation of their importance as secondary triggering factors of other hazards, such as slope sedimentary instabilities and tsunamis.

4.2. Submarine Slope Instabilities

Sedimentary instabilities are common processes in all submarine environments, where the largest slope instabilities in the Earth occur [70] (Figures 1 and 4). They may be classified according to different approaches, such as mechanical behavior, particle support mechanisms, sediment concentrations, and longitudinal changes in their deposits, or according to the relationship between source areas, dimensions, and geometries of deposits [71–76]. Based on the mechanical properties and rheology of the processes, two main groups can be defined: (i) slides/slumps/spreads and (ii) gravity flows. These two groups, with important differences in their pre- and post-failure behavior, occur in all physiographic environments and are efficient transporters of sediment, organic carbon, nutrients, and pollutants [77–81]. They are scale-invariant processes that range greatly in size from the meter scale to many km across (Figure 4).

Slides/slumps are movements of sediment or rock along a surface of rupture that develops in a layer with low shear strength or a weak layer [82]. They are elastoplastic movements that include translational and rotational movements (Figure 4a–c). Spreads, the submarine characterization of which has increased during the last decade, are sediment or blocks of consolidated sediment moving over liquefied underlying material and not a basal shear plane [83]. Depending on the mechanical behavior or the energy available, all these mentioned movements of sediments may evolve into a sediment flow, but a flow may also develop directly if the sediment is completely remolded.

A wide range of flow types can occur because of the interplay of rheology, grain size composition, and concentration (Figure 4). Flows in general have viscoplastic behavior and can be divided into cohesive (e.g., mud flows and debris flows) (Figure 4d) and non-cohesive flows (grain flows), depending on the amount of fine-grained matrix [84]. One type of cohesionless flow involving large volumes of failing masses is debris/rock avalanches. Usually, such failures originate from deep rotational failures on high-gradient slopes and in volcanic environments [85]. Turbidity currents are a type of Newtonian flow in which fluid turbulence is key to supporting the sediment and keeping it in suspension. Turbidity currents can transport up to hundreds of cubic kilometers of sediment at high velocities (up to 19 m/s) over thousands of kilometers [33,86] (Figure 4c).

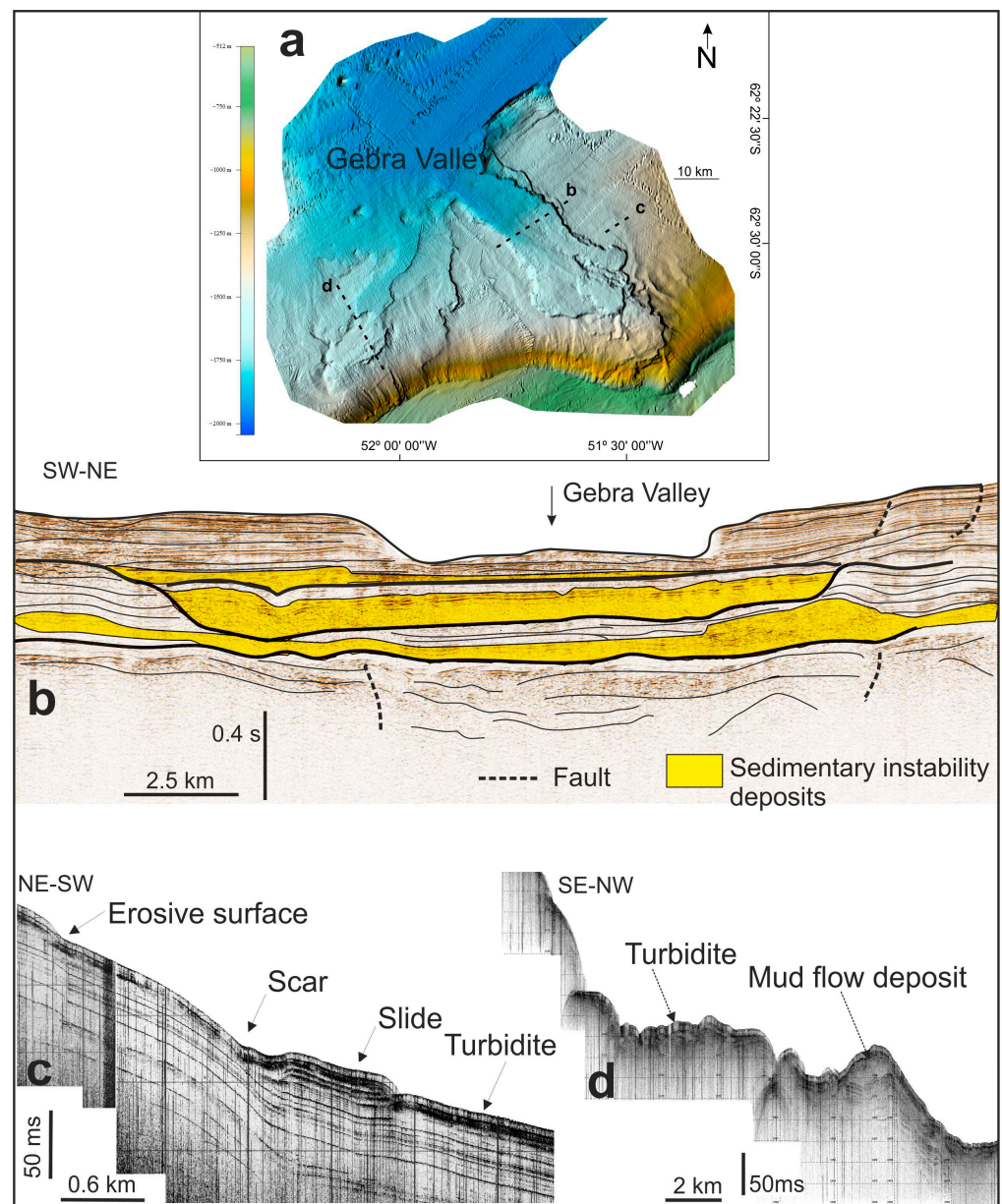


Figure 4. Examples of submarine slope instabilities: (a) multibeam bathymetry displayed in the Gebra Valley area, Bransfield Basin (Antarctic); more details regarding this valley can be found in [87]. The dashed lines show the cross-sections of seismic records in b, c, and d; (b) Airgun seismic record displaying the repeated large-scale slope failure events that were responsible for the cut-and-fill features forming the Gebra Valley; (c,d) parametric seismic records showing the different slope instabilities affecting the external margins of the Gebra Valley; more details on those slope instabilities in [88].

Field monitoring of turbidity currents has increased in recent years. However, these processes and failures are still primarily recorded in nature, and most of the knowledge acquired is through the interpretation of the resulting geomorphology and the study of the final deposits. This situation leaves unanswered key questions and uncertainties about all the mechanisms involved in sedimentary instabilities, which need further study. These questions will have to be addressed at different scales through repeated very high-resolution bathymetric surveys, high-resolution (and 3D) seismic surveys, new direct deep-sea monitoring and mobility sensors, in situ geotechnical tests, and experimental and numerical models. Better field observations and models will help to achieve an

improved understanding of numerous aspects, such as the rates of seafloor changes, the role of preconditioning factors, the impact of triggers, how rapidly a slope failure can develop, and the volumes of sediment involved and reworked. Improved knowledge of the governing mechanisms, evolution, and transformation of these submarine sedimentary instabilities will be crucial to understanding the hazard they represent [89–94]. Their modelling will also help to assess their consequences.

When landslide hazard assessment is considered, concepts such as distribution, time, and magnitude must be considered [95–97]. Regional inventories and magnitude-frequency relationships, including events triggered over a long period of time or almost instantaneously, could provide critical information [98]. Nevertheless, accurate chronological constraints (ideally combining biostratigraphic and radiometric techniques) will be essential for hazard evaluation.

4.3. Submarine Volcanism

Volcanoes are vents in the Earth's crust through which molten rock, hot rock fragments, and gases can erupt. Magma can rise along conduits to the surface, forming lava that either continuously flows out or shoots upward. Furthermore, the lava can break into pieces that are thrown into the air or into the sea due to decompression of the gases it contains (<https://www.britannica.com/science/volcano>, accessed on 3 September 2020).

From a marine point of view, volcanic eruptions affecting the sea water column can be grouped into four basic types (Figure 5):

- (i) Subaerial eruptions close to the coastline affect the marine environment in different ways, as they can produce changes in the coastal configuration when lava flows pour into the sea forming a lava delta (e.g., [99]) (Figure 5b), collapse the volcanic edifice, or enter the sea of pyroclastic flows (e.g., [100]) (Figure 5a). Moreover, volcanic eruptions and dike intrusions can even cause slope sedimentary instabilities that enter the sea and trigger tsunami waves (e.g., [101] and references therein).
- (ii) Shallow-water eruptions (<200 m water depth, mwd) are commonly characterized by violent explosions, especially when they approach the water-air interface (Figure 5c), as observed for the first time at Surtsey in 1963 [102].
- (iii) Intermediate-water eruptions (approximately 300–600 mwd) are rarely observed, but they can be characterized by a peculiar eruptive style characterized by floating lava balloons or pumice emissions (Figure 5d). During these eruptions, lava globes can be expelled in a successive way that occurred in the recent submarine eruptions of Serreta (Terceira, Azores; [103] or Tagoro (Canary Islands) (Figure 5e).
- (iv) Deepwater eruptions (>600 mwd) are mostly effusive, and the associated lavas represent the most widespread surficial igneous rocks on Earth. Related studies have focused on basaltic lavas emplaced in mid-oceanic ridges, back-arc basins, intraplate seamounts, ocean volcanic islands, and plateaus. Three main types of submarine lavas can be distinguished according to their morphology and flow rates: pillow, lobate, and sheet [104,105]. For basaltic lavas, another important deposit is hyaloclastite occurring in both shallow and deep waters. The 2012 Havre eruption exhibited explosive activity in a deep-water sector (between 900 and 1100 mwd), producing a pumice raft approximately 400 km² in size and an abundance of fine ash on the seafloor over the course of one day [106].

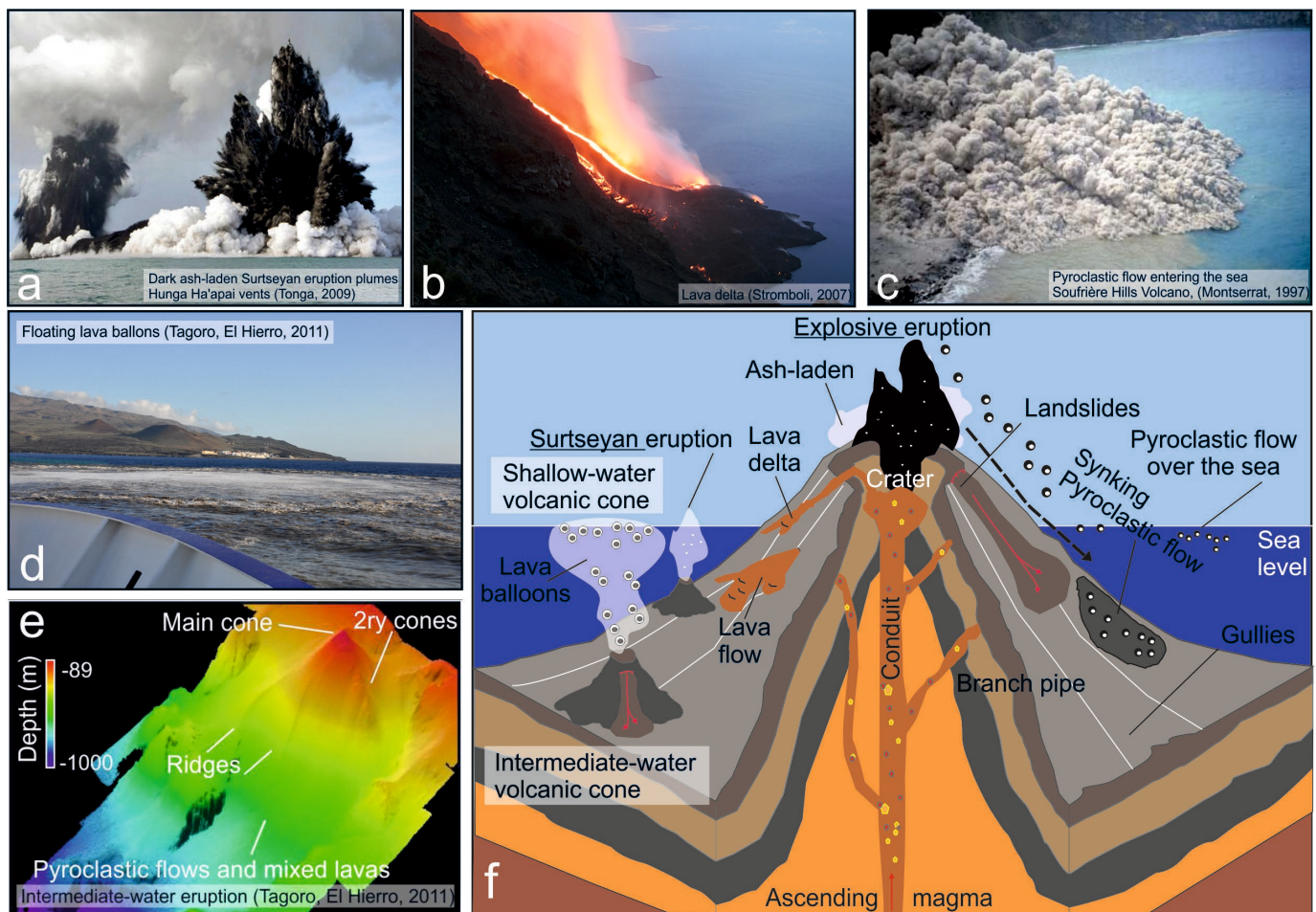


Figure 5. Main types of eruptions examples: (a) Sinking pyroclastic flows in Montserrat island (image from <https://www.pinterest.com/pin/398709373236700178/>, accessed on 2 November 2020); (b) emplacement of the 2007 lava delta at Stromboli (image from <https://www.swisseduc.ch/stromboli/volcano/sciara0203/delta-growth-2007-it.html?id=5>, accessed on 5 October 2020); more details on the 2007 submarine eruption can be found in [107,108]; (c) Surtseyan eruption plumes from Hunga Ha'apai vents (Tonga) in 2009 (image from <https://volcano.si.edu/>, accessed on 5 October 2020); (d) floating volcanoclastic materials and gas emissions during the Tagoro volcanic eruption offshore El Hierro in 2011; more details on this submarine eruption can be found in [109]; (e) 3D bathymetric map of the Tagoro volcano showing the main morphological characteristics; (f) 3D simplified sketch of the main types of eruptions affecting insular volcanoes.

Another important hazardous phenomenon associated with volcanic eruptions that can become a hazard is gas emissions. The most common volcanic gases are water vapor, carbon dioxide, carbon monoxide, sulfur dioxide, and hydrogen sulfide; to a lesser extent, methane, hydrogen, helium, nitrogen, hydrogen chloride, or hydrogen fluoride can also be emitted (<https://www.britannica.com/science/volcano>, accessed on 1 October 2020). These gas emissions can cause loss of life due to suffocation if they reach the surface and can kill fauna present in the environment surrounding the underwater eruption. Such eruptions can also induce strong acidification of seawater, resulting in the subsequent loss of habitats around the eruption. For example, in the eruption of the Tagoro volcano, the pH dropped to 5, and the partial pressure of dissolved carbon dioxide increased almost 1000 times [108,110].

Despite the large number and volume of submarine volcanic eruptions, our understanding of such processes and associated landforms is still limited, especially compared with their subaerial counterparts ([111–113] and reference therein). Many concepts are still based on the interpretation of ancient deposits and on theory (e.g., [114] and references therein). However, the growing availability of detailed digital elevation models (also used

to depict seafloor changes associated with eruptions through repeated surveys) integrated with hydroacoustic monitoring and in situ observations of volcanic settings will exponentially increase their detection (considering that volcanic eruptions only occasionally reach the sea surface) and our knowledge of submarine eruptive processes (e.g., [115–120]).

A challenge-based study will provide knowledge to understand the processes that take place in the evolution of a submarine volcano at different depths. The main effort should focus on monitoring these processes using a variety of instrumentation (including on-land seismometers and marine stations with OBSs, hydrophones, pressure sensors, CTD (conductivity, temperature, and depth) instruments, and geochemical parameter sensors to control emissions) to allow study of the eruptive pulses and the content of emissions. Some of this instrumentation will be able to be connected by optical cables to laboratories onshore for online monitoring (e.g., [121]), and profiles can be made with a towed oceanographic rosette (tow-yo). Another challenge will be understanding the changes in seafloor morphology through time-lapse high-resolution bathymetry surveys, taking advantage of the use of autonomous underwater vehicles (AUVs) for deep volcanoes.

4.4. Fluid Flow Processes

Seepage is a global process that occurs in different geodynamic contexts in both active and passive continental margins. Generally, this process includes the leakage of hydrocarbons (particularly methane as both dissolved and free gas), water, and/or sediment [21,122] (Figure 6). The gas in shallow marine sediments [123,124] is mainly composed of methane, and its origin is attributed to either biogenic or thermogenic processes. The escape of fluid from the sediment may occur as micro-seeps or as sudden violent escapes (cold seeps), producing diverse types of morphologies on the sea floor (Figure 6a) or in the subsurface [21]. Some features have positive relief (e.g., mounds, methane-derived authigenic carbonate, gas hydrates, mud volcanoes), and others have negative topographies on the seafloor (e.g., pockmarks, collapses) (Figure 6). Gas can migrate through unlithified sediments along bedding planes, faults, and fractures (Figure 6b) driven by buoyancy forces and pressure gradients [125,126]. Glacial-isostatic and tectonic events may reactivate fractures and faults, producing temporal variability in spatially heterogeneous fluid flow [127].

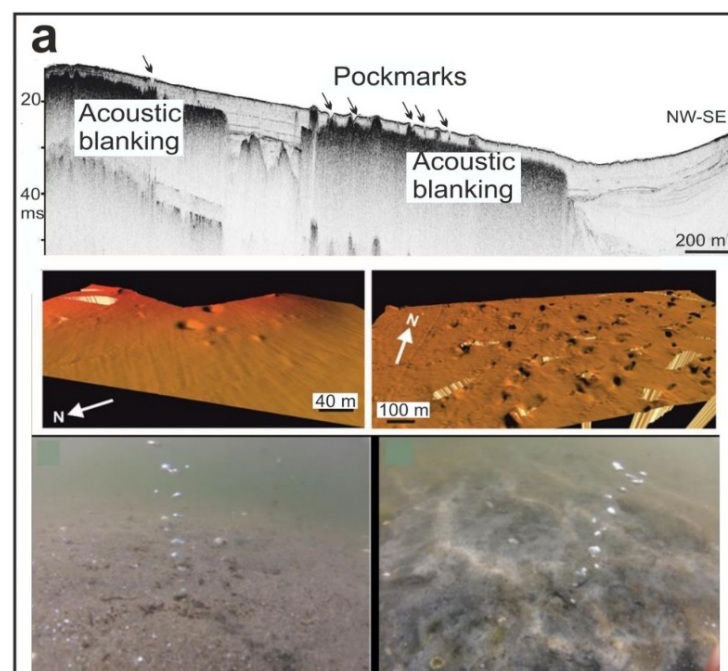


Figure 6. Cont.

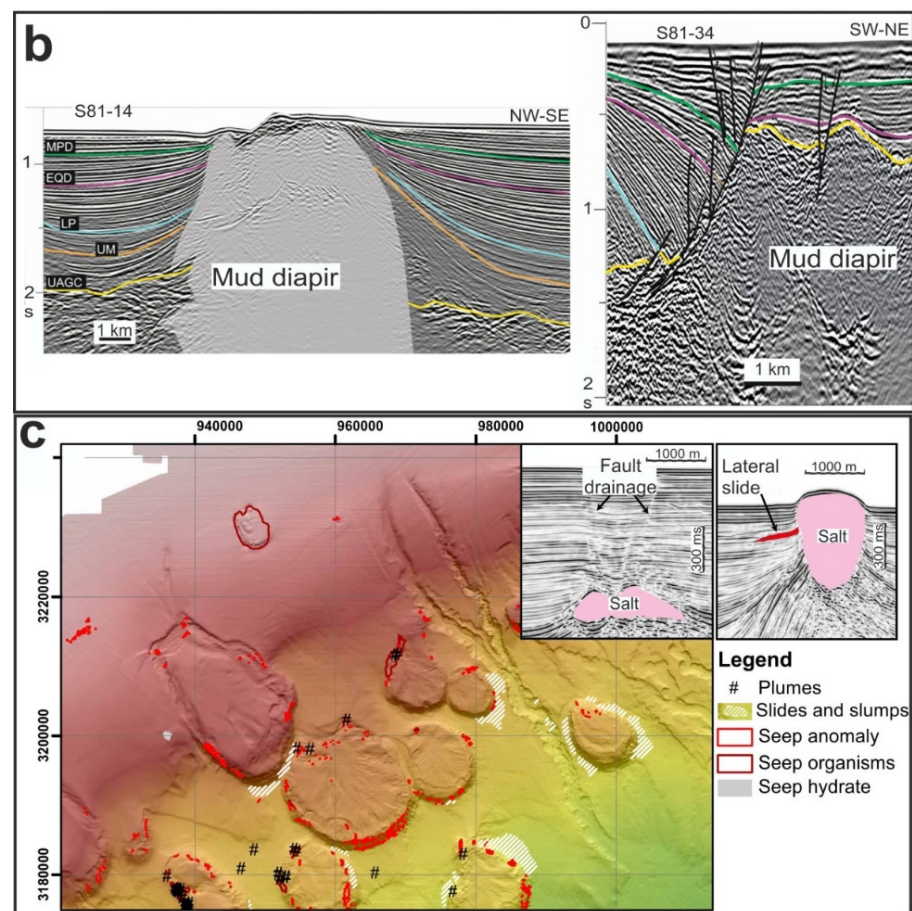


Figure 6. Examples of hazardous features related to fluid flow processes: (a) At the top: very high-resolution seismic profile (3.5 kHz) in the Ria de Vigo showing an acoustically blank zone related to the presence of shallow gas accumulations near the seabed (less than 1 meter below the seabed). It also shows the presence of pockmarks and the main paths of gas escape. In the middle: multibeam echosounder images from Ría de Vigo displaying depressions related to gas escapes (pockmarks) and mounds formed by the accumulation of debris (mud and bivalve shells) from mussel rafts. At the bottom: methane-gas bubbles escaping from the sandy and muddy seabed of the Ría de Vigo; (b) mud diapirs related to the compressive regime (left figure) and to listric faults (right figure); (c) high-resolution bathymetric map of the northeastern Gulf of Mexico showing salt diapirs (rounded positive structures) piercing the seafloor and their associated seep anomalies associated with oil and gas seepages, slides and slumps, and gas hydrates to a lesser extent (images from <https://www.boem.gov/oil-gas-energy/mapping-and-data/map-gallery/boem-northern-gulf-mexico-deepwater-bathymetry-grid-3d>; accessed on 15 September 2020; <https://www.boem.gov/oil-gas-energy/mapping-and-data/map-gallery/seismic-water-bottom-anomalies-map-gallery>, accessed on 16 September 2020; https://metadata.boem.gov/geospatial/WBA_Metadata.xml, accessed on 16 September 2020); more details on the northeastern Gulf of Mexico salt diapirs in [128,129]). Enclosed seismic records show: a detailed view of salt-related normal faults acting as drainage pathways for deep fluids and lateral slides associated with overburden salt diapirs in a 2D seismic line located in the Gulf of Lion, western Mediterranean Sea.

The mud fluidization and degassing processes associated with overpressure contribute to the formation of mud volcanoes. This fluidization is mainly due to the overpressure generated by tectonic stresses or by lithostatic pressure in regions with high sedimentation rates [130]. These types of structures are one of the most important methane sources in the hydrosphere and atmosphere [131–133]. Diapirs are gravitational/tectonic structures

(Figure 6b) produced mainly by salt, clays, or a mix of these lithologies that, currently, have little consideration in submarine hazard models. These intrusive bodies of relatively low density tend to migrate upward, deforming and piercing the overlying sedimentary sequences. They can appear with other fluid migration structures, such as mud volcanoes or pockmarks. In an extensive context, the development of diapirs commonly occurs close to deep listric faults (Figure 6b) that act as escape migration routes. The formation of mud diapirs is more frequent in compressive settings, as highly over-pressurized diapiric material (e.g., [134]) can move upward from subsurface depths up to 3–4 km to the seafloor. In various tectonic regimes, diapir activity may also trigger slope instabilities (Figure 6c) because the deformation and elevation of these structures favor seafloor oversteepening and seismicity [135].

Gas hydrate is an ice-like crystalline solid form of water and low molecular weight gas (e.g., methane, ethane, and carbon dioxide) [136]. Methane hydrates can form at any depth where the geothermal conditions are colder than the hydrate stability curve. This occurs in the upper hundred meters of marine sediment at water depths greater than 500 m. Nevertheless, certain conditions, such as the presence of saline pore waters or clays, can inhibit gas hydrate formation, while a high fluid flux can promote gas hydrate formation [137,138]. Seismic reflection techniques are used to determine the areal extent of gas hydrates in marine locations mainly by the identification of bottom-simulating reflectors (BSRs) (e.g., [139]). However, gas hydrates have been recovered from sites without BSRs. This is because the saturation of methane hydrate in the pore space must exceed approximately 40% for the seismic velocity to be altered significantly enough to generate a BSR [140]. Gas hydrates may be a significant hazard because they alter sea floor sediment stability and can lead to collapses and landslides that may trigger tsunamis [141–145], and their breakdown and release to the water column and atmosphere may have a strong influence on the environment and climate [146].

The presence of all these fluid flow features usually denotes subsurface hydraulic activity, over-pressurization, fluidization, and degassing processes, as well as sudden fluid (gas and/or liquid) release that may produce gas explosions, slope sedimentary instabilities, and an uplifting/subsiding seafloor [122,147–149] (Figure 6c). These processes can have major impacts on seabed infrastructures and on those requiring piles that are driven into the seafloor. Therefore, it will be necessary to extend systematic investigations to identify the locations of fluid dynamic processes in areas where their activity remains unknown currently. Thus, heat flow studies will need to be increased in order to detect and map new subseafloor marine fluid flows and understand their regimes. High-resolution 3D seismic surveys will also allow an accurate acoustic characterization and distribution assessment of the different fluid dynamic features and definition of their origins. They also have the potential to document and characterize in more detail the different types and timing of deformation patterns in areas close to diapirs and related mud volcanoes, with the goal of accurately determining the timing of fluid flow processes. Additionally, studies on microseismicity would allow the detection of fluid injection. Monitoring of fluid flows should also increase in active cold seeps; systematic sediment and gas sampling for biogeochemical analysis will aid the understanding of the general physical and geochemical characteristics of the escaping gas. Likewise, improved numerical models of gas hydrate formation, stability, quantification, and role in the shear strength of the host sediment will lead to progress in understanding the impact of gas hydrates on safety and seafloor stability.

4.5. Bottom Currents

The term “bottom currents” refers to all persistent currents flowing near the seabed that resuspend, transport, and/or control sediment deposition [150]. Although bottom currents are semipermanent features, they are characterized by high variability over a range of time scales (from daily to geological timescales; [151]). They may occur in shelf, slope (Figure 7) and deep basin settings. In shelf settings, wind and tidal forcings are common

and produce different hydraulic regimes (e.g., tide- and current-dominated regimes). In deep-water settings, bottom currents are mostly related to thermohaline circulation. These currents are driven by density gradients (e.g., the North Atlantic Deep Water) and typically flow subparallel to the bathymetric contours with velocities of 1–20 cm/s [152]. In particular settings (e.g., narrow gateways), bottom currents strongly intensify, reaching velocities of 50–300 cm/s (e.g., the Mediterranean outflow water that spills over the Gibraltar sill, e.g., [153,154]). In deep-water settings, submarine canyons can be swept by focused tidal currents with up and down flows and velocities of 25–50 cm/s [142]. Moreover, an increasing number of studies (e.g., [142,155–158]) have highlighted that several intermittent oceanographic processes can affect the seabed: eddies, gyres, helical flows, benthic storms, cascading dense shelf water, internal waves, and currents related to extreme, cyclonic, and tsunami waves.

As most of these processes can produce complex flow conditions, an increase in the velocity of bottom currents and additional shear stress may produce considerable sediment resuspension and seabed erosion [155] (Figure 7f–g). All these observations highlight that a variety of oceanographic processes are able to exert a significant impact on shaping the seafloor when bottom currents are active for a prolonged period of time (Figure 7a). At small spatial scales, they generate various erosional and depositional bedforms, ranging in size from centimeters to kilometers (see, e.g., [151,159]) (Figure 7c,f–h) and whose identification is particularly relevant for geohazard assessments of seabed infrastructure. At a larger scale, bottom currents with persistent activity on a geological time scale (e.g., thermohaline-induced currents) may form regionally extensive contourite depositional systems [158,160–163], including a variety of depositional elements (contourite drifts) (Figure 7a) and erosional elements (contourite channels, furrows, moats, and erosive terraces).

Evaluating the action of bottom currents is crucial for hazard assessment because intense seabed erosion may locally favor slope instability [164] (Figures 7a–e,i). Moreover, migrating bedforms (e.g., sand waves) and erosion (Figure 7f–h) can have major impacts on seabed infrastructure [7]. This can be extremely relevant in narrow straits swept by powerful tidal currents and by internal waves (e.g., the Messina Strait) that can create a dangerous setting for submarine cables and pipelines [165]. Other crucial areas are canyons swept by strong tidal bottom currents, topographic highs (e.g., seamounts and ridges) where bottom currents interact with topography [163,166–168], areas affected by tidal forcing and associated internal waves [169], areas of local upwelling [170,171], seasonal fluctuations in the main circulation pattern [172], or areas of sinking dense water [173], which may trigger slope sedimentary instabilities (e.g., [174,175]). Finally, it is noteworthy that contourite deposits can be prone to becoming unstable (e.g., [176]), as several predisposing factors (e.g., mounded morphology on steep slopes and the low shear strength related to high sedimentation rates) may favor slope failures [22] (Figure 7i).

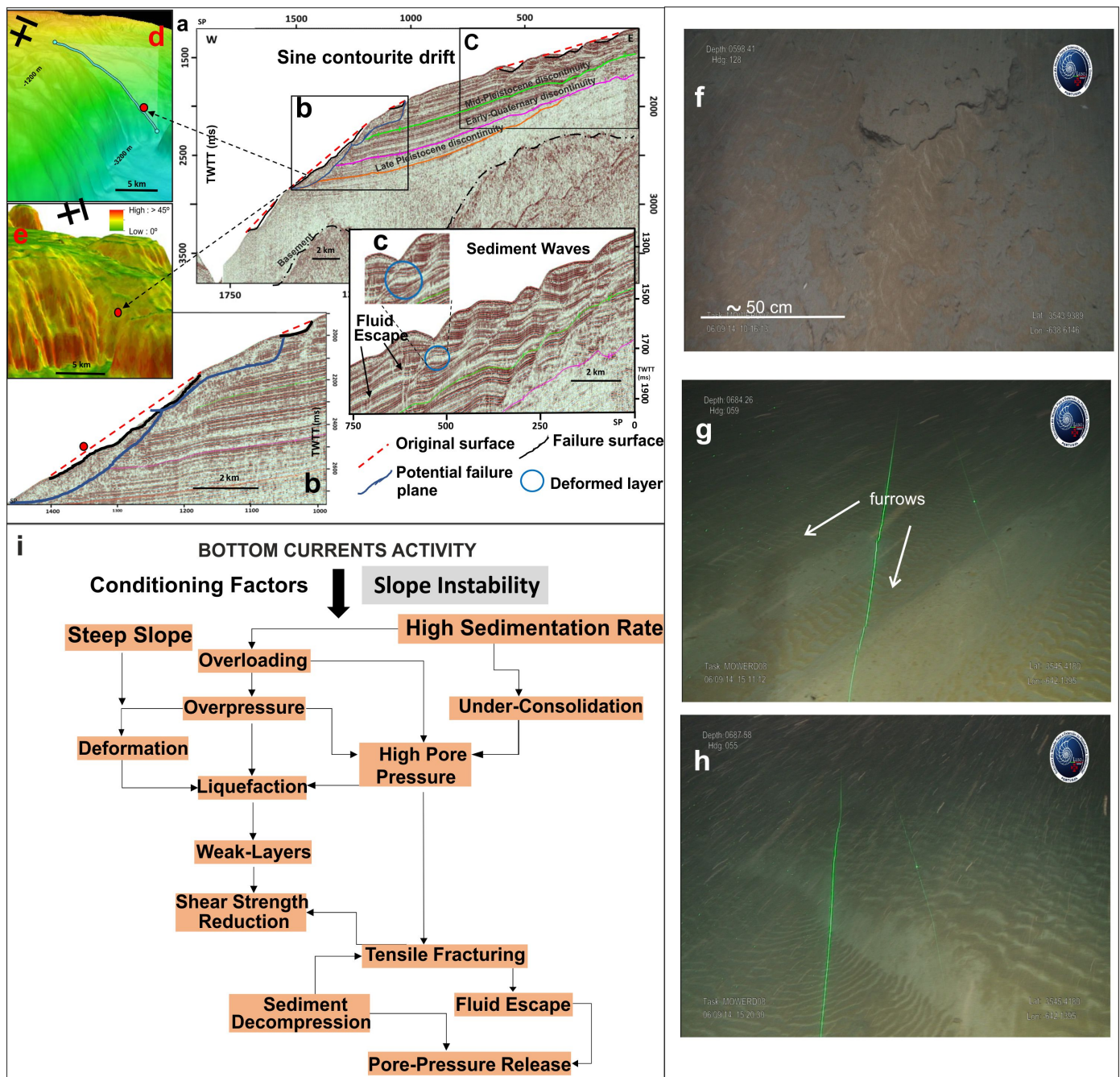


Figure 7. Examples of hazardous features related to bottom current action of the Mediterranean outflow water around Iberia: **(a)** Sines contourite drift (Portugal margin, NE Atlantic) is affected by slide scars on the seafloor and failure surfaces in the subsurface. Additionally, upslope-migrating sediment waves occur in the near-surface sediments; **(b)** details of slide scars and potential failure surfaces; **(c)** details of sediment waves; **(d)** details of the bathymetric map with the track of the seismic profile shown in **(a)**. The red dot marks the headscarp of a landslide scar; **(e)** detail of the slope gradient map; **(f-h)** ROV images showing bedforms in the continental slope of the Gulf of Cadiz (NE Atlantic): **(f)** Indurated muddy outcrop (grey in color) indicates intense current flow erosion; the mudstone is covered partially by sand with ripples. The two laser lines are separated 50 cm; **(g)** erosive furrows excavated on the muddy seafloor, covered partially by sandy sediment with starved rectilinear to sinuous asymmetric ripples. This starvation allows for the exposure of the mudstone surface over which the ripples are moving; **(h)** sinuous sand wave with superimposed linguoid to sinuous asymmetrical ripples on the stoss side and rectilinear to sinuous ripples in the trough area. The two laser lines are separated 50 cm; **(i)** diagram showing the intrinsic and hazardous properties of contourite deposits that may contribute to slope failures. Figure 7a-e,i was adapted with permission from [158]. Copyright 2019, Elsevier.

Recognition of the potential hazard of deep-water bottom currents is increasing because new and large seafloor areas of contourites have intensively eroded during the last 15 years due to mobile seafloors and slope sedimentary instabilities, which have been mapped (e.g., [150,155,158,160,162,177]). The assessment of the role of bottom current activity as a hazardous process is challenging for geoscientists due in part to the need to establish a dialogue with physicist oceanographers (e.g., [162]); as it is necessary to define flow conditions, induced bed shear stress and effects on morpho-sedimentary processes affecting the seabed, as well as their evolution over time. Thus, a multidisciplinary approach, including oceanographic, morphologic, sedimentologic, stratigraphic, and geotechnical studies, should be used. This will require multidisciplinary surveys and the integration of complex datasets, including oceanographic data (CTDs, acoustic Doppler current profilers (ADCPs), and transmissometers to measure the water properties and velocity not only at the near-bottom but also throughout the water column), multibeam bathymetry data, sub-bottom profile data, seafloor samples, sediment cores, and remotely operated vehicle (ROV) videos. Data integration enabled characterization of the different oceanographic processes, their interactions and timing, and their influences on the near-bottom flows acting on the seafloor. AUV surveys will also be required for high-resolution geophysical surveys in deep-water environments. Repeated bathymetric surveys and seafloor observatory systems will be required to define seabed evolution over time. Finally, hydrosedimentary modelling will be very helpful in assessing seabed changes and bed shear stress over a defined time period (e.g., the lifetime of the infrastructure).

4.6. Tsunamis

The main mechanisms for tsunami generation are earthquakes caused by seismogenic fault movement (96% of events), slope sedimentary instabilities, and volcanic eruptions (Table S1). In addition, with the release of large volumes of gas from seafloor sediment, atmospheric disturbances (meteotsunamis), or even cosmic impacts can also produce tsunamis [178] (Figure 8). Finally, anthropogenically induced submarine slope sedimentary instabilities have triggered local tsunamis [179]. To perform tsunami hazard assessment, three main components of the phenomena must be addressed: the generating mechanism, wave propagation in the open sea, and coastal inundation.

Seismotectonic tsunamis are triggered by the coseismic vertical displacement of the seafloor impacted by an earthquake and the transmission of this movement to the water column [180,181] (see Video S1 in the Supplementary Materials). Normal fault movement causes the water masses to sink toward the formed depression, generating an initial large sine wave at the surface of water mass (Figure 8a). In contrast, reverse faults move the seafloor upward, and the water column is pushed upward (Figure 8b), forming an initial large crest wave on the sea surface. Tsunami wave generation by seismotectonics is controlled by the rupture velocity (mostly slow velocities), fault type, slip and average vertical displacement, width, length, and segmentation of the rupture zone of the fault in the seafloor [181].

Submarine slope instabilities (such as slumps, slides, debris/rock avalanches, debris flows) generally involve large volumes of sediments and rocks, and the associated movement within the water body generates a dipole-like water wave that can eventually generate major tsunami waves [15,182–184]. The initial shape of the tsunami wave is defined by a depression–uplift pair in the water surface (Figure 8c). The water depression is due to the sudden sediment vacuum that occurs at the slide scar (Figure 8c, number 1), which becomes occupied by sea water, and the uplift (Figure 8c, number 2) is due to the pressure force exerted upwards by the fast-moving slide material. Several aspects of submarine slope instabilities as tsunami sources are currently being discussed, namely, the rheology (because it influences the deformation of the sliding material during their runout) [84,85], acceleration, and volume. These aspects are considered to be key factors controlling the geometry (depression and uplift) of the generated tsunami wave [185].

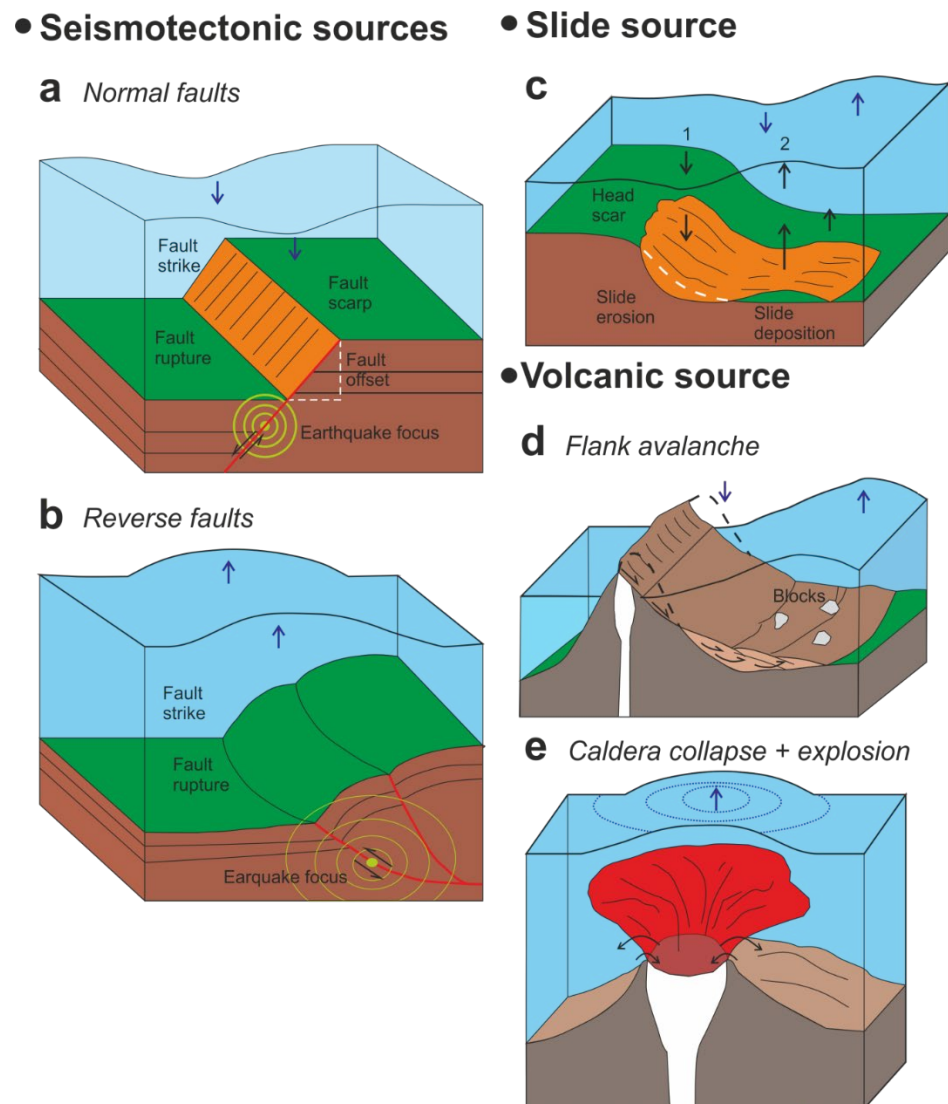


Figure 8. Sketch of the main tsunamigenic sources of geological origin: (a) Normal fault activity; (b) reverse fault activity; (c) submarine landslide. Numbers 1 and 2 refer to the time-sequenced development of the initial tsunami shape in the water surface; (d) collapse flanks of volcanoes; (e) volcanic explosion related to eruptions and caldera collapses.

Volcanic eruptions can also induce subaerial and submarine slides, slumps, debris/rock avalanches, or debris flows on the flanks of volcanoes that, in turn, can produce tsunami waves (Figure 8d) and they can also generate caldera explosions that can cause the complete collapse of the edifice [186–188]. These explosions produce waves (Figure 8e) that are generated first by the explosion itself and then by the sinking of the volcanically mobilized material.

Tsunami waves move in all directions from the source area, affecting the entire water column [189]. Their initial propagation, especially their direction, is conditioned by the geometric and deformation characteristics of the source structure. Tsunami waves are initially characterized by their large wavelengths (tens or hundreds of kilometers), small heights in the open sea (on the scale of centimeters), and large velocities. The wave velocity is greater in deeper waters (700 km/h at depths > 4000 m), and when depth decreases, the velocity also decreases to 30–50 km/h at the coast. Simultaneously, the wavelength decreases and the wave increases in height to balance the kinetic energy with potential energy (e.g., [190]).

Tsunamis can have significant impacts on coastal communities, depending on regional and local bathymetry and coastal geomorphology variability [191,192]. The occurrence of reefs, human infrastructure, the geometry of the coastline and beaches, and the presence of bays, estuaries or deltas at river mouths can influence the size, appearance, and impact of tsunamis when they arrive at the coast. Typically, a tsunami reaches the coast as a series of successive crests and valleys, sometimes separated by several or tens of minutes, and can reach the coast as a rapid flood, more rarely as a wall of water, or, sometimes, as an initial withdrawal of the sea (e.g., [178]). Thus, the destruction caused by a tsunami on the coast can be very different at relatively short distances. The long wavelength of tsunamis gives them more momentum such that they can flood areas hundreds of meters and even kilometers from the coast. The maximum height above sea level that a tsunami reaches on the coast is known as the runup and mostly ranges from 1 m to 30 m, with extreme heights > 500 m, as in the case of the tsunami that occurred in Lituya Bay [184], when the coast is very close to the source area or where the coastal geomorphology amplifies the tsunami effects (resonant effects) (e.g., [181]).

The challenges in tsunami hazard research should focus on several aspects. First, an accurate definition of tsunamigenic sources is needed because it will help reduce the uncertainty in the triggering mechanism and will be important for studying the events themselves (e.g., the frequency of reoccurrence, potential areas to be impacted). Other aspects should include establishing their recurrence intervals by identifying past events in sediment cores (palaeoearthquakes, palaeoslides, and palaeotsunamis), and applying in situ measurements plus long-term monitoring. For seismotectonic sources, faults have to be described in terms of their tectonic style, dynamics, present-day activity, fault zone geometry, fault offsets of sedimentary units, and fault surface. For slope sedimentary instability-generated tsunamis, knowledge of the seafloor geometry, slope failure processes, and their early post-failure evolution is fundamental to determining their triggering potential. To analyze these concerns, high- and ultrahigh-resolution bathymetric data and 3D seismic reflection profiles, in situ seismicity measurements and observations, long-term monitoring, and longer sediment cores will be fundamental.

Additional challenges that will also be important for studying tsunami events and their impacts include the development of increasingly realistic mathematical models of the tsunami generation process, propagation through the water masses, and the impact on the coastal zones and the establishment of tsunami early warning systems (TEWSs). This work will include increasing the model resolution, developing more efficient and faster than real-time (FTRT) codes, and using future exa-scale computational architectures. Probabilistic tsunami hazard analyses (PTHAs) will have to be conducted in different areas of the world at global, regional, and even local scales with the aim of understanding tsunami hazards and developing tsunami risk reduction activities. PTHA increases the knowledge of the potential tsunamigenic threats at different scales by estimating the probability of exceeding specific levels of tsunami metrics, such as the maximum inundation height or runup within a certain period of time, around determined locations. Furthermore, probabilistic tsunami forecasting (PTF) attempts to address the uncertainty in tsunami forecasts by formulating a probability density function (PDF). The use of PTF in the context of rapid hazard assessment and in TEWSs is also a major challenge.

5. Scenarios with Multiple Geological Hazards

Following the above arguments and characteristics, the understanding of the different geohazard factors also needs to recognize the distribution of the main hazardous features, how they can interact, and their potential to generate cascading events. The most common of this type of event comprises an earthquake that triggers a landslide, both of which can produce a tsunami. Additionally, bottom currents can scour an overstepped seafloor, thereby reducing the shear strength of the unaffected sediments upslope and leading to their failure, forming a landslide that may produce a tsunami. Furthermore, the breakdown of sub-bottom gas hydrates can increase the pore pressure of the sediment bearing the

released gas, which may lead to tsunamigenic slope sedimentary instability. Despite the highly scattered distribution of these factors along continental margins, they commonly coincide in certain specific environments or geological contexts, which should be monitored by the scientific community. Diverse settings, such as fjords, active river prodeltas, canyon-fan systems, subduction areas, or even high-latitude open slopes, may be critical. Among them, three settings are highlighted for their multiple hazardous features.

5.1. Tectonic Indentation Areas

Tectonic indentation areas in marine settings are significant because the tectonic structures developed in a framework of continental collision. The consequences of this tectonic activity are the presence of source areas that can produce multiple geohazards, such as earthquakes, sedimentary instabilities and, to a lesser extent, tsunamis. The continental indentation structures in marine areas occur in convergent continental margins related to plate corners (Taiwan, [193]) and accretionary wedges (Manila Trench, [194]) and in areas of early continental collision, such as the westernmost Mediterranean (Alboran Sea, [195]; Aguilas Arc in the Gulf of Vera, [196]). Particularly, the central Alboran Sea and the Aguilas Arc/Gulf of Vera (Figure 9) are key areas for understanding the link between indentation and geological hazards in a land–marine transition context; this is because although both exhibit similar hazardous features (seismic faults and slope instability deposits), their degree of development is different. Continental indentation influences the tectonics of the adjacent oceanic areas, as occurs during the northward indentation of the Arabian plate in Eurasia, which determines the westward motion of the Anatolian Block related to the development of the Aegean Sea [197]. The indenter blocks are generally bounded by lateral seismogenic strike-slip faults that permit displacement during the process of collision [198].

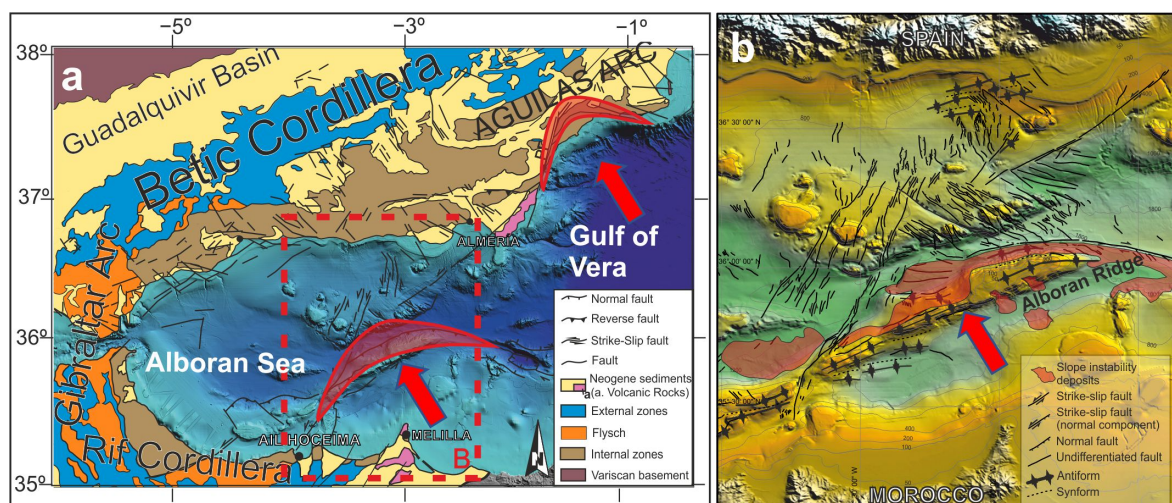


Figure 9. Example of multiple geological hazards in a tectonic indentation area in the western Mediterranean: (a) Geologic map showing the main tectonic features of the westernmost Mediterranean and the tectonic indentation zones in the central Alboran and Aguilas Arc in the Gulf of Vera; (b) detailed tectonic features of the Central Alboran Basin (for more details see [195]) and areas of generalized slope instability deposits (red areas). Legend: the red arrow indicates the direction of tectonic indentation and the red shading indicates the location of tectonic indentation.

Indentation structures simultaneously develop fault sets, folds, and block tilting, which can generate submarine slope sedimentary instabilities. These structures require integrated analysis by 3D analogue modelling, which has improved over time from early models [198] to recent models [199]. Future research will need to determine the stage of development of tectonic indentations. Additionally, the future development of new generations of numerical modelling is required. Another key question to address in the study of marine indentation zones is the tsunamigenic potential of strike-slip-related faults. In general, this type of fault is not considered tsunamigenic because it does not

significantly displace the seafloor. However, new data in the central Alboran Sea contradict this theory and indicate the need to investigate other strike-slip faults in similar geological frameworks [195].

5.2. Canyon Heads Close to Coast

Submarine canyons, especially their shallower parts, are commonly very active geomorphological features that should be highlighted because of their association with multiple hazards (e.g., [200–202]). In general, canyons are located on the edge between a continental shelf and the continental slope, but some excavate the shelf to the point that their heads are only a few hundred meters from coastal towns, for example, the Garrucha (Figure 10a,e) and Gioia canyons in the Mediterranean [97–198,203,204] and the Congo and Capbreton canyons in the eastern Atlantic [19,205]. In these scenarios, changes can occur due to interactions among coastal processes (deposition and erosion) (e.g., [205]), river discharge (e.g., [206]), oceanographic processes (e.g., [207]), and seismicity related to tectonic processes (e.g., [208]). These activities can also produce favorable conditions for sedimentary instabilities (Figure 10a–d), which may produce tsunamis. Likewise, canyon heads close to the coast strongly influence tsunami propagation and runup (e.g., [209]).

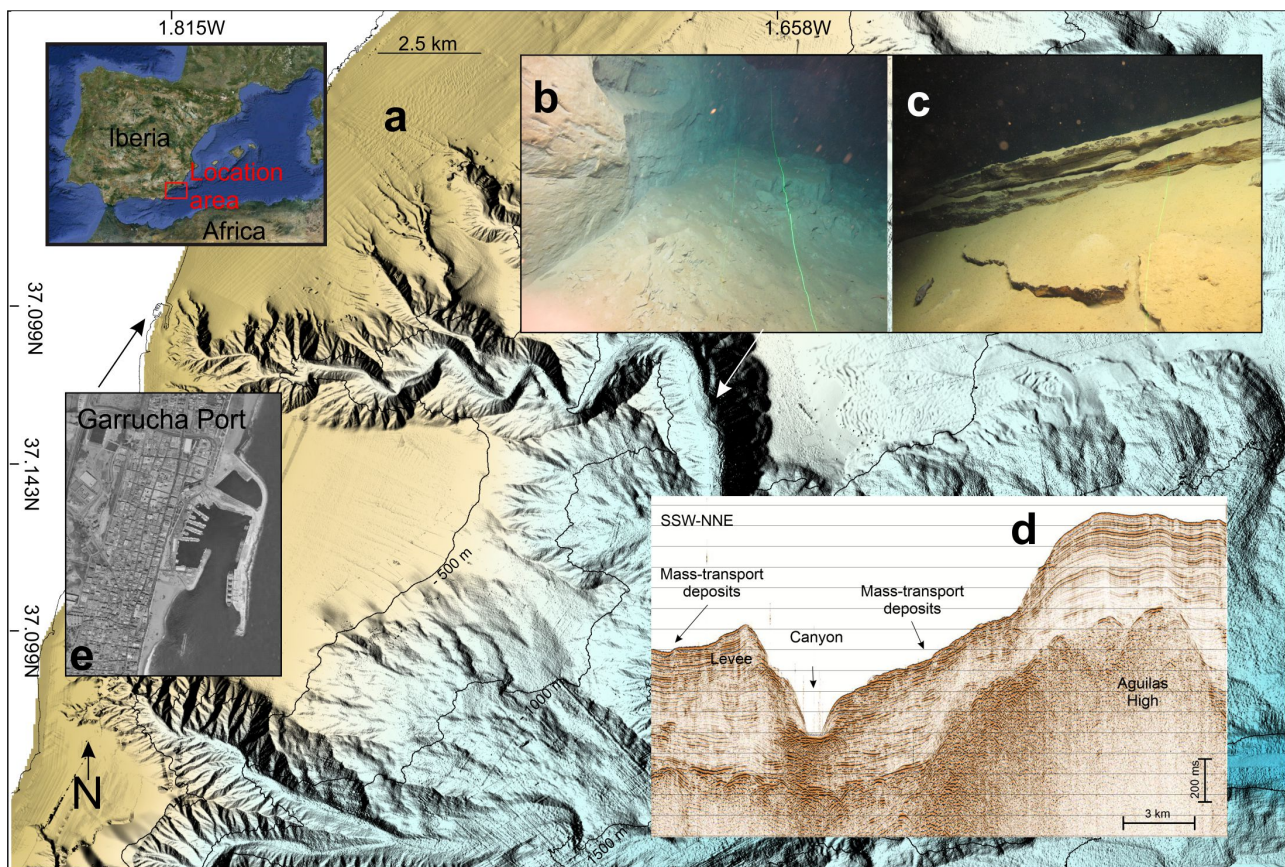


Figure 10. Example of multiple geological hazards in the Garrucha Canyon, SW Mediterranean: (a) Bathymetric map displaying a canyon head affected by intense gullying of its two main tributaries; (b,c) ROV (remotely operated vehicle) images displaying slope failures affecting the canyon walls; (d) seismic profile illustrating the occurrence of mass-transport processes that contribute to the erosion of the canyon walls; (e) photograph of the Garrucha port, which is located at the canyon head, where the sedimentary instability processes that contribute to canyon-head retrogradation affect its pier.

Therefore, key scientific issues to be addressed include obtaining a better understanding of each submarine and coastal geological process and the oceanographic and climatic processes that govern the retrogradation, incision, and enlargement of canyon heads (e.g., [210]). To achieve this goal, detailed 2D, 3D, and 4D geomorphological vi-

sualization will be needed. This work should be carried out not only at the head of the canyons but also in the adjacent areas of the continental shelf, open continental slope, and infralittoral zone (Figure 10a). This visualization will allow us to typify and map with high precision the different morphological elements (both erosive and depositional) of the integrated canyon-head-margin system [101]. Within the canyon heads, the morphometric, chronostratigraphic, sedimentological, and geotechnical characterizations of submarine slope instabilities will be crucial; the integrated results will allow us to estimate the recurrence of events and to assess and model the potential canyon-head stability [204]. New insights will be fundamental to establishing the spatiotemporal relationship between slope sedimentary instabilities, tectonics, and oceanography and to defining areas that may be prone to failure (e.g., [211]).

5.3. Volcanic Islands

Volcanic islands and their submarine portions merge multiple geohazards, mainly associated with volcanic eruptions, flank collapses, slope instabilities (Figures 5a–e and 11), and associated tsunamis, although strong volcano-tectonic subsidence [212], retrogressive erosion at canyon heads [213,214], and earthquake swarms (e.g., [215]) deserve special attention for hazard assessment. Flank collapses and slope instabilities ([216] and reference therein) (Figures 5g and 11) represent a common hazardous process during the evolution of many insular volcanoes, which are often able to mobilize volumes up to thousands of cubic kilometers (e.g., [186,217–219]). For instance, the 100–400 × 10⁶ m³ flank collapse affecting Anak Krakatau in 2018 generated a tsunami with a runup of up to 13 m along the Sunda Strait. Despite the high tsunamigenic potential associated with these large-scale events, their hazard is relatively low because they have recurrence times on the order of thousands of years. In contrast, small- and medium-sized slope instabilities affecting active volcanic flanks are more hazardous because they have markedly shorter recurrence times and are able to generate local but devastating tsunamis [220,221]. One of the best examples is recognizable at Stromboli Island, where five tsunamigenic landslides over just the last century have been reconstructed [222]. In the case of highly explosive eruptions, the entrance of pyroclastic currents into the sea can also generate tsunami waves or travel (their upper and dilute parts) over the sea for distances of tens of kilometers before impacting surrounding coastal communities, as described during the 1883 Krakatoa eruption [223].

Considering the multiple often closely related hazards affecting volcanic islands, the key scientific recommendation for an effective hazard assessment in such areas should include the use of an integrated and multidisciplinary approach encompassing both the submarine and subaerial flanks of the island. High-resolution mapping will be fundamental to understanding the variability in volcanic edifices and associated landforms (Figure 11) and to performing systematic parametrization to provide insights into the complex interplay between the volcanic, tectonic, erosive-depositional, and eustatic processes (for shallow-water areas) that control the genesis of volcanic islands ([113] and references therein). This mapping (Figure 11) will also be the basis for planning more detailed surveys with seismic methods, ROV dives, and seafloor sampling and for successive bathymetric comparisons aimed at understanding what occurs during eruptive crises. In this regard, the availability of multiple time-lapse bathymetric surveys has been proven to be a very effective tool for monitoring seafloor changes associated with volcanic and/or failure events occurring in both shallow water (e.g., [107,115,224]) and deep water (e.g., [225,226]). In particular, the integration of repeated bathymetric surveys with acoustic monitoring and/or ROV dives will increase our ability to detect and understand eruption dynamics in submarine environments [120,227,228].

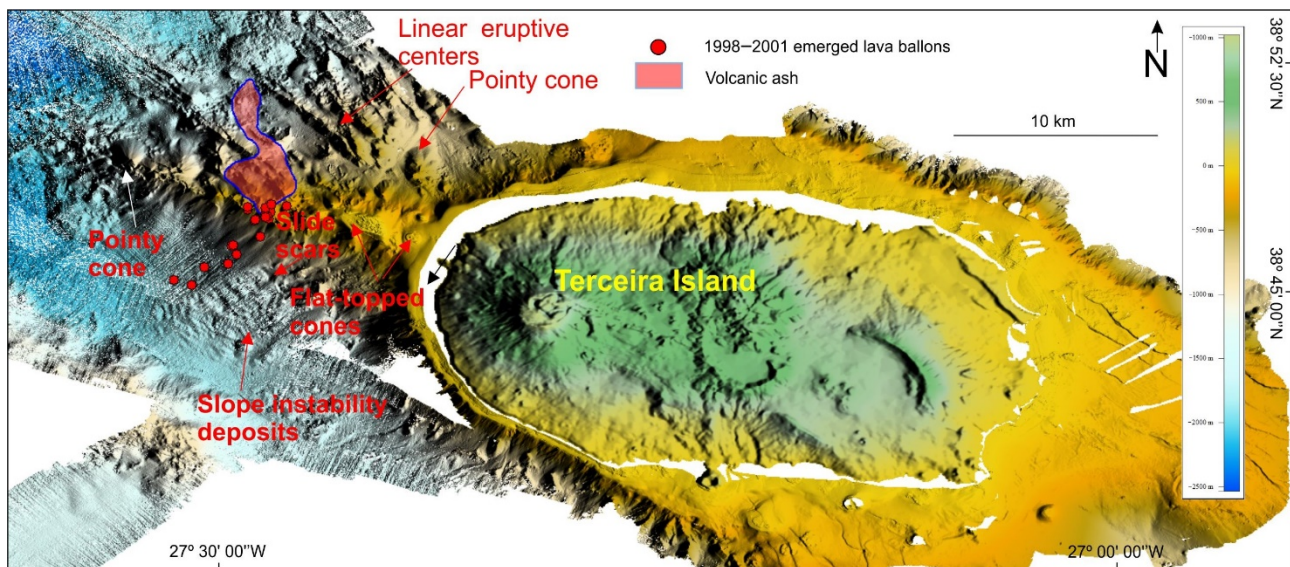


Figure 11. Main characteristics of Terceira Island (Azores; North Atlantic Ocean) and the bathymetry surrounding the island. The map also shows the area where lava balloons clusters and volcanic ash were observed at the sea surface during the 1998–2001 Serreta eruptions; more details on these eruptions can be found in [118,229].

6. Conclusions: A Distinctive Multidisciplinary Approach to Study Offshore Geological Hazards

Offshore geological hazards include convulsive and persistent geological processes and are mainly represented by seismicity, slope sedimentary instabilities, submarine volcanism, fluid flows, and bottom currents; tsunamis are also mentioned because they are commonly a secondary hazard generated mostly by earthquakes, slope instabilities, or volcanic eruptions. They can occur in any domain or environment in the oceans and seas and represent a real and serious threat to society, the economy, and the environment.

Despite the progress in data acquisition and the establishment of evolutionary models for the different hazardous features, each dedicated section has identified knowledge gaps and how these gaps can be addressed. We also note that hazardous processes can interact and potentially generate cascading events.

This review establishes that the challenges for improving outcomes in offshore geohazard research can be addressed with multidisciplinary approach studies. This approach requires cross-disciplinary research to bring together multiscale analysis, mapping, direct deep-sea observations and testing, and modelling in scenarios with individual, but mainly multiple geohazards. This approach will lead to multicriteria decisions for understanding hazardous processes and their causative factors.

A qualitative step in the multiscale analysis involves the acquisition of long-term geological records, such as seismic profiles with different degrees of resolution and penetration and geophysical data (e.g., magnetometer and gravimeter data) (Figure 12), all acquired simultaneously in surveys using emerging technology and applying advanced tools for processing and geophysical modelling (Figure 12). The long-term records also provide the opportunity to study seismic profiles and sediment cores (the longer the better) (Figure 12) to improve our understanding of the magnitude and frequency of hazardous processes. Advancing techniques in sediment core analysis and age dating will contribute to reducing the uncertainty between stratigraphic correlations and increase their temporal resolution. This will facilitate the attainment of more accurate information about the sediment age and the recurrence interval of hazardous events. The success of these observations from these conventional but continuously advancing techniques will be closely tied to seafloor mapping, direct deep-sea observations and testing, and modelling.

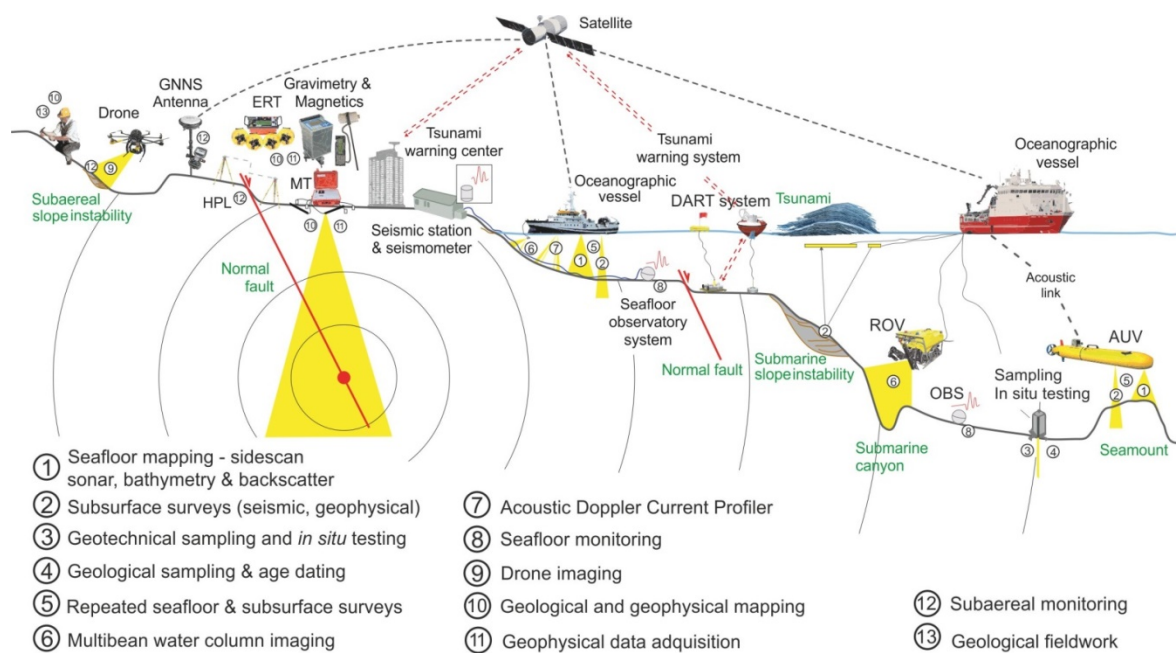


Figure 12. A distinctive methodological approach to study offshore geological hazards. The main future directions for studying offshore geohazards will be the implementation of multiscale and multidisciplinary approaches joining conventional and emerging tools for monitoring, mapping, direct observations, in situ testing, and modelling. Scenarios can be affected by multiple hazardous features, some in a land-marine transition context, and the integration of offshore and onshore observations is essential. The figure was used as idea and base to create a new one including more information from [79].

Mapping is not a new approach but is still needed to fill the existing gaps along many continental margins and basinal plains and to provide higher-resolution seafloor maps from shallow to deep-sea areas, thus providing more details on the occurrence of hazardous features. This task is mandatory for taking the next step in geological hazard assessment. The capacity to perform repeated high-resolution multibeam bathymetric surveys is also a very effective tool for monitoring seafloor changes, and it has to be implemented for a better understanding of hazardous processes. In this sense, the use of AUVs with multibeam sonars and sub-bottom profilers in repeated surveys and of ROVs for direct observations are essential to map the active hazardous seafloor features with maximum resolution, even in deep sea environments (Figure 12); the temporal resolution of their mapping will be important to report their dynamic evolution. Seismic record acquisition also plays an important role in mapping prior hazardous processes. In this sense, a greater use of 3D seismic data is expected to offer new and unprecedented sub-bottom geomorphologic information, enabling an accurate delimitation and characterization of active structures, especially in complex geological settings. However, the success of future efforts to map hazardous seafloor features will require confident geomorphological models and mapping standards for the correct understanding and recognition of features. There is still a long way to go before the scientific community reaches an agreement on standards for marine geohazard mapping, but this is a requirement for future multiple hazard maps and catalogues.

Direct observations and testing are also technical challenges because both are linked to the development of new sensors, techniques, protocols, and infrastructures, such as seafloor observatories (Figure 12). The development of new seafloor observatory systems with capabilities and facilities for remote and real-time recording over long periods of time will lead to qualitative advances. Direct observations of active structures and measurements of smaller-scale, but highly recurrent, events will enhance our understanding of larger processes and also provide important data for small-scale models. Moreover, direct observations and measurements from the water column via the optimization of

mooring systems, CTDs, ADCPs, and transmissometers will be essential to understand the physics of the environment (e.g., bottom currents, turbidity, etc.). Additionally, direct seafloor monitoring by seafloor network systems, including OBSs with longer standing periods than are available in the present and DART (Deep-ocean Assessment and Reporting of Tsunamis) buoy systems, or the use of submarine cables to detect earthquakes, will provide better seismic data with which to define active faults, surface ruptures, volcanic activity, and tsunamis (Figure 12). Direct seafloor observations and measurements, together with inland seismic stations, will allow us to define seismogenic and aseismic faults and estimate realistic peak ground acceleration (PGA) values, which depend on the epicentral distance and earthquake magnitude (Figure 12). Seismic loading is critical to defining the factor of safety (F) and the susceptibility to slope failure of different seafloor areas. Integrated seafloor and inland monitoring will be a key element to increase the reliability and timeliness of the information used by early warning systems (Figure 12). However, future generations of AUVs and ROVs, which have become more widely accessible to the scientific community and easier to manage, will also provide new opportunities for in situ sampling of sediments, monitoring the rate of seafloor mobility, fluid seepage characterization, and measuring in situ geotechnical parameters. The in situ geotechnical properties (Figure 12) involve the goal of obtaining contact measurements (seafloor and sub-bottom) using advanced static (e.g., cone penetrometer, pressuremeter, heat flow), dynamic (e.g., XBP) and combined systems. The measurement of the dynamic effect of seismic events or other cyclic sources, such as storm waves and internal waves on the sediment, especially on the pore pressure, is another rarely performed technical approach that will need to be enhanced (e.g., dynamic simple shear tests). Special in situ tests can reveal the real effect of high sedimentation rates or fluid flow dynamics (gas emissions) on the sediment and its geomechanical characteristics. In addition, in situ geotechnical property measurements will be closely tied to the assessment of potential seafloor stability by the application of probabilistic methods, for which GIS is an adequate and very powerful tool.

The success of future efforts for an effective seismic hazard assessment will be reliant on new and better geological models taking advantage of developments in artificial intelligence. Consequently, the future of the field of geohazards is coupled to enhanced computational capabilities. This is also because this field will face a massive volume of datasets (i.e., the so-called big data problem). Datasets will be generated from new hull-mounted and towed methodological instruments as well as autonomous and permanent observational systems recording multiple hazard datasets with higher temporal and spatial resolution. This means that in the future, a common but key challenge will be the ability to efficiently manage and analyze (also in real time) massive data; therefore, the need to train geoscientists and build the capacity to operate advanced computational systems are needed. Massive data linked to the advances in artificial intelligence will open new lines of research for the use of advanced deep learning and machine learning algorithms, for example, for automatic detection and classification of different variables (e.g., slope gradients, roughness, backscatter signal amplitudes, grain size, density) involved in the identification of geohazard features. The development of complex neural networks trained to detect variables of interest (e.g., in seismograms, bathymetries, cores) will offer an important advancement both qualitatively (elements could be detected automatically that could go unnoticed by the most trained analyst) and quantitatively (the analysis of multiple datasets as well as their spatiotemporal relationships will increase exponentially). Such advances will lead to a much greater understanding of hazardous processes and will have significant effect on the probabilistic methods for assessing geological hazards with more robust models from which early warning systems will benefit.

Furthermore, there is also the need to enhance multidisciplinary studies in the geological scenarios with multiple hazardous processes that can interact and generate cascading events. These scenarios can be affected by hazardous features that are connected from sea to land. Therefore, the integration of on-land information, e.g., Global Navigation Satellite System (GNSS), high-precision levelling, seismicity monitoring, multiple geophysical

datasets (including magnetometer, gravimeter, magnetotelluric (MT), electrical resistivity tomography (ERT), and HPL data, and field, drone, and satellite Earth observations), with submarine results is critical to realizing the correct assessment of hazards (Figure 12). In this sense, scientific and technical coordination of the research community working on subaerial and submarine hazardous structures with different datasets is a major task that is still in its infancy, and reinforcement is required in the future.

Supplementary Materials: The following are available online at <https://www.mdpi.com/article/10.3390/oceans2020023/s1>, Table S1: Okada’s parameters [3] describing the two fault segments involving of the Horseshoe and Marques de Pombal faults as source for the tsunami modelling. Video S1: NIVEL0_MDPHORSE.

Author Contributions: Conceptualization, G.E. and D.C. (David Casas); Writing—original draft: all authors based on their geological hazard expertise; Introduction by G.E. and D.C.; Human activities and historical cases and by G.E. and B.A.; Definition and classification of geohazards by G.E. and D.C. (David Casas); Tectonic earthquakes by J.G.-Z., F.E., L.G.-C., A.M.-T., and V.T.-S.; Landslides by D.C. (David Casas), M.A.-Z., and J.I.-G.; Volcanism by D.C. (Daniele Casalbore), O.S.-G., and J.-T.V.; Tsunamis by J.-T.V., J.M., J.M.G.-V., and D.P.; Fluid-flow by S.G.-G., D.D., M.C.F.-P., and G.E.; Bottom currents by E.M., M.T., and C.J.; Scenarios involving multiple geological hazards by G.E., D.C. (David Casas), D.C. (Daniele Casalbore), F.E., and J.G.-Z.; Conclusions by G.E., D.C. (David Casas), J.N., J.V., and M.Y.; Integration—review-reediting: G.E. and D.C. (David Casas). All authors have read and agreed to the published version of the manuscript.

Funding: This study was supported by the following scientific projects: FAUCES (MINECO/FEDER, CMT2015-65461-C2-R), DAMAGE (MINECO/FEDER, CGL2016-80687-R); B-RNM-301-UGR18, P18-RT-3275 and RNM148 from Junta de Andalucía; GRACE (Eurofleets: EFP_SEA02-024); VULCANO (CTM2012-36317); RIGEL (IEO); MEGAFLOW (MEC/FEDER, RTI2018-096064-B-C21); and CHEESE (UE (H2020-INFRAEDI-2018-1, PROJECT ID: 823844). This study was also carried out in the framework of the IGCP 640-S4LIDE. In addition, the research was also conducted in collaboration with the Andalusian PAIDI Research Group RNM 328 (Coastal and Marine Geology and Geophysics).

Acknowledgments: The ICM-CSIC authors acknowledge Severo Ochoa funding from the Spanish government through the “Severo Ochoa Centre of Excellence” accreditation (CEX2019-000928-S). We also thank IHS-Markit for the Kingdom Suite educational license. This article is dedicated to the memory of Albert Figueras, who devoted the last years of his life as director of the UTM-CSIC.

Conflicts of Interest: The authors declare no conflict of interest.

References

- Bell, F.G. *Geological Hazards: Their Assessment, Avoidance and Mitigation*; CRC Press: Boca Raton, FL, USA, 2003.
- Nadim, F. Challenges to geo-scientists in risk assessment for submarine slides. *Nor. J. Geol.* **2006**, *86*, 351–362.
- Hough, G.; Green, J.; Fish, P.; Mills, A.; Moore, R. A geomorphological mapping approach for the assessment of seabed geohazards and risk. *Mar. Geophys. Res.* **2011**, *32*, 151–162. [[CrossRef](#)]
- Ercilla, G.; Casas, D. *Submarine Mass Movements: Sedimentary Characterization and Controlling Factors*; Intech: London, UK, 2012.
- Chiocci, F.L.; Cattaneo, A.; Urgeles, R. Seafloor mapping for geohazard assessment: State of the art. *Mar. Geophys. Res.* **2011**, *32*, 1–11. [[CrossRef](#)]
- Neumann, B.; Vafeidis, A.T.; Zimmermann, J.; Nicholls, R.J. Future coastal population growth and exposure to sea-level rise and coastal flooding—A global assessment. *PLoS ONE* **2015**, *10*, e0118571. [[CrossRef](#)] [[PubMed](#)]
- Camargo, J.; Silva, M.; Ferreira, J.A.; Araújo, T. Marine geohazards: A bibliometric-based review. *Geosciences* **2019**, *9*, 100. [[CrossRef](#)]
- Campbell, K.J. Deepwater geohazards: How significant are they? *Lead. Edge* **1999**, *18*, 514–519. [[CrossRef](#)]
- Yonggang, J.I.A.; Chaoqi, Z.H.U.; Liping, L.I.U.; Dong, W. Marine geohazards: Review and future perspective. *Acta Geol. Sin.* **2016**, *90*, 1455–1470. [[CrossRef](#)]
- Bouma, A.H. *Offshore Geologic Hazards: A Short Course Presented at Rice University, May 2–3, 1981 for the Offshore Technology Conference*; Bouma, A., Sangrey, D., Coleman, J., Prior, D., Trippet, A., Dunlap, W., Hooper, J., Eds.; American Association of Petroleum Geologists: Tulsa, OK, USA, 1981; Volume 18, pp. 48–101.
- Bates, R.L.; Jackson, J.A. *Glossary of Geology*; American Geological Institute: Alexandria, VA, USA, 1987.
- Ayala, F.J. *Introducción a Los Riesgos Geológicos. En IGME (1988) Riesgos Geológicos; Serie Geología Ambiental; Instituto Geológico y Minero de España (IGME): Madrid, Spain, 1998.*

13. Calarco, M.; Zolezzi, F.; Johnson, W.J. Offshore Geohazards-Industry Implications and Geoscientist Role. In Proceedings of the Near Surface Geoscience 2014—20th European Meeting of Environmental and Engineering Geophysics, Athens, Greece, 14–18 September 2014; European Association of Geoscientists & Engineers: Houten, The Netherlands, 2014; pp. 1–5.
14. Camerlenghi, A. Addressing Submarine Geohazards Through Scientific Drilling. In Proceedings of the EGU General Assembly 2009, Vienna, Austria, 19–24 April 2009; Center for Astrophysics: Vienna, Austria, 2009; p. 3151.
15. Harbitz, C.B.; Løvholt, F.; Bungum, H. Submarine landslide tsunamis: How extreme and how likely? *Nat. Hazards* **2014**, *72*, 1341–1374. [[CrossRef](#)]
16. Sassa, S.; Takagawa, T. Liquefied gravity flow-induced tsunami: First evidence and comparison from the 2018 Indonesia Sulawesi earthquake and tsunami disasters. *Landslides* **2018**, *16*, 195–200. [[CrossRef](#)]
17. Espuela, J.A.; Ercilla, G.; Farran, M.L. Submarine erosion in North Spanish Atlantic sea. *Hydro Int.* **2005**, *9*, 54–57.
18. Keller, E.A.; Pinter, N. *Active Tectonics*; Prentice Hall: Upper Saddle River, NJ, USA, 1996.
19. Cooper, C.K.; Wood, J.; Andrieux, O. Turbidity Current Measurements in the Congo Canyon. In Proceedings of the Offshore Technology Conference, Houston, TX, USA, 6–9 May 2013; pp. 1–12.
20. Carter, L.; Gavey, R.; Talling, P.; Liu, J. Insights into Submarine geohazards from breaks in subsea telecommunication cables. *Oceanography* **2014**, *27*, 58–67. [[CrossRef](#)]
21. Hovland, M.; Judd, A.G. *Seafloor Pockmarks and Seepages, Impact on Geology, Biology and the Marine Environment*; Graham & Trotman: London, UK, 1988.
22. Laberg, J.S.; Camerlenghi, A. Chapter 25 The Significance of Contourites for Submarine Slope Stability. In *Developments in Sedimentology*; Rebesco, M., Camerlenghi, A., Eds.; Elsevier: New York, NY, USA, 2008; Volume 60, pp. 537–556.
23. Carter, L. *Submarine Cables and the Oceans: Connecting the World (No. 31)*; UNEP/Earthprint: Nairobi, Kenya, 2010.
24. Halfar, J.; Fujita, R.M. Precautionary management of deep-sea mining. *Mar. Policy* **2002**, *26*, 103–106. [[CrossRef](#)]
25. Benn, A.R.; Weaver, P.P.; Billet, D.S.M.; van den Hove, S.; Murdock, A.P.; Doneghan, G.B.; Le Bas, T. Human activities on the deep seafloor in the North East Atlantic: An assessment of spatial extent. *PLoS ONE* **2010**, *5*, e12730. [[CrossRef](#)] [[PubMed](#)]
26. Dunbar, P.; McCullough, H.; Mungov, G.; Varner, J.; Stroker, K. 2011 Tohoku earthquake and tsunami data available from the National oceanic and atmospheric administration/National geophysical data center. *Geomat. Nat. Hazards Risk* **2011**, *2*, 305–323. [[CrossRef](#)]
27. Fritz, H.M.; Petroff, C.M.; Catalán, P.A.; Cienfuegos, R.; Winckler, P.; Kalligeris, N.; Weiss, R.; Barrientos, S.E.; Meneses, G.; Valderas-Bermejo, C.; et al. Field survey of the 27 February 2010 Chile tsunami. *Pure Appl. Geophys.* **2011**, *168*, 1989–2010. [[CrossRef](#)]
28. Hawkes, A.D.; Bird, M.; Cowie, S.; Grundy-Warr, C.; Horton, B.P.; Hwai, A.T.S.; Law, L.; Macgregor, C.; Nott, J.; Ong, J.E.; et al. Sediments deposited by the 2004 Indian ocean tsunami along the Malaysia-Thailand Peninsula. *Mar. Geol.* **2007**, *242*, 169–190. [[CrossRef](#)]
29. Galindo-Zaldivar, J.; Ercilla, G.; Estrada, F.; Catalán, M.; d’Acremont, E.; Azzouz, O.; Casas, D.; Chourak, M.; Vazquez, J.T.; Chalouan, A.; et al. Imaging the growth of recent faults: The case of 2016–2017 seismic sequence sea bottom deformation in the Alboran sea (Western Mediterranean). *Tectonics* **2019**, *37*, 2513–2530. [[CrossRef](#)]
30. Meschis, M.; Roberts, G.P.; Mildon, Z.K.; Robertson, J.; Michetti, A.M.; Walker, J.F. Slip on a mapped normal fault for the 28th December 1908 Messina earthquake (Mw 7.1) in Italy. *Sci. Rep.* **2019**, *9*, 6481. [[CrossRef](#)]
31. Stover, C.W.; Coffman, J.L. *Seismicity of the United States, 1568–1989 (Revised)*; U.S. Geological Survey Professional Paper; U.S. Government Printing Office: Washington, DC, USA, 1993.
32. Brune, S.; Ladage, S.; Babeyko, A.Y.; Müller, C.; Kopp, H.; Sobolev, S.V. Submarine landslides at the eastern Sunda margin: Observations and tsunami impact assessment. *Nat. Hazards* **2009**, *54*, 547–562. [[CrossRef](#)]
33. Genesseeux, M.; Mauffret, A.; Pautot, G. Les glissements sous-marins de la pente continentale niçoise et la rupture de câbles en mer ligure (Méditerranée Occidentale). *Comptes Rendus l’Académie Sciences Paris* **1980**, *290*, 959–962.
34. Dan, G.; Sultan, N.; Savoye, B. The 1979 nice harbour catastrophe revisited: Trigger mechanism inferred from geotechnical measurements and numerical modelling. *Mar. Geol.* **2007**, *245*, 40–64. [[CrossRef](#)]
35. Piper, D.J.W.; Shor, A.N.; Clarke, J.E.H. The 1929 “grand banks” earthquake, slump, and turbidity current. In *Sedimentologic Consequences of Convulsive Geologic Events*; Clifton, H.E., Ed.; Geological Society of America: Boulder, CO, USA, 1988; Volume 229, pp. 77–92.
36. Bugge, T. Submarine slides on the Norwegian continental margin with special emphasis on the storegga slide. *IKU Rep.* **1983**, *110*, 1–152.
37. Bryn, P.; Berg, K.; Stoker, M.S.; Haflidason, H.; Solheim, A. Contourites and their relevance for mass wasting along the Mid-Norwegian margin. *Mar. Pet. Geol.* **2005**, *22*, 85–96. [[CrossRef](#)]
38. Bondevik, S.; Løvholt, F.; Harbitz, C.; Mangerud, J.; Dawson, A.; Svendsen, J.I. The Storegga slide tsunami—Comparing field observations with numerical simulations. *Mar. Pet. Geol.* **2003**, *22*, 195–208. [[CrossRef](#)]
39. Forte, G.; De Falco, M.; Santangelo, N.; Santo, A. Slope stability in a multi-hazard eruption scenario (Santorini, Greece). *Geosciences* **2019**, *9*, 412. [[CrossRef](#)]
40. Wyss, M. A proposed source model for the great Kau, Hawaii, earthquake of 1868. *Bull. Seismol. Soc. Am.* **1988**, *78*, 1450–1462.
41. Carracedo, J.C.; Torrado, F.P.; González, A.R.; Soler, V.; Turiel, J.L.F.; Troll, V.R.; Wiesmaier, S. The 2011 submarine volcanic eruption in El Hierro (Canary islands). *Geol. Today* **2012**, *28*, 53–58. [[CrossRef](#)]

42. Hildenbrand, A.; Marques, F.O.; Catalão, J. Large-scale mass wasting on small volcanic islands revealed by the study of Flores island (Azores). *Sci. Rep.* **2018**, *8*, 13898. [[CrossRef](#)] [[PubMed](#)]
43. Hovland, M. Seabed pockmarks on the Helike detal front. In *Ancient Helike and Aigialeia, Proceedings of the Second International Conference, Aigion, Greece, 1–3 December 1995*; Katsonopoulou, D., Schildardi, D., Soter, S., Eds.; Helike Society: Athens, Greece, 1995; pp. 461–471.
44. Worzel, J.L.; Watkins, J.S. Location of a Lost Drilling Platform. In *Proceedings of the Offshore Technology Conference, Houston, TX, USA, 5–7 May 1974*; pp. 771–772.
45. Brook, H.; Cook, R.; Harris, J. Competitive concrete gravity base foundation for offshore wind farm. In *Coast, Marine Structured and Breakwater, Adapting to Change*; Allsop, W., Ed.; Thomas Telford Books: London, UK, 2010; pp. 62–73.
46. Whitehouse, R.J.S.; Sutherland, J.S.; O'Brien, D. Seabed Scour Assessment for Offshore Windfarm. In *Proceedings of the 3rd International Conference on Scour and Erosion, Gouda, The Netherlands, 3–5 July 2007*; pp. 1–320.
47. Dahlberg, R. Observations of scour around offshore structures. *Can. Geotech. J.* **1983**, *20*, 617–628. [[CrossRef](#)]
48. Demars, K.R.; Vanover, E.A. Measurement of wave-induced pressures and stresses in a sandbed. *Mar. Geotechnol.* **1985**, *6*, 29–59. [[CrossRef](#)]
49. Herbich, J.B. Hydromechanics of submarine pipelines: Design problems. *Can. J. Civ. Eng.* **2011**, *12*, 863–874. [[CrossRef](#)]
50. Lubick, N. Earthquakes from the ocean: Danger zones. *Nature* **2011**, *476*, 391–392. [[CrossRef](#)]
51. Bird, P.; Kagan, Y.Y.; Jackson, D.D. Plate tectonics and earthquake potential of spreading ridges and oceanic transform faults. In *Plate Boundary Zones*; Stein, S., Freymueller, J.T., Eds.; AGU: Washington, DC, USA, 2002; pp. 203–218.
52. Beeson, J.W.; Johnson, S.Y.; Goldfinger, C. The transtensional offshore portion of the northern San Andreas fault: Fault zone geometry, late pleistocene to holocene sediment deposition, shallow deformation patterns, and asymmetric basin growth. *Geosphere* **2017**, *13*, 1173–1206. [[CrossRef](#)]
53. Barnes, P.M.; Sutherland, R.; Delteil, J. Strike-slip structure and sedimentary basins of the southern alpine fault, Fiordland, New Zealand. *Geol. Soc. Am. Bull.* **2005**, *117*, 411–435. [[CrossRef](#)]
54. Frohlich, C.; Apperson, K.D. Earthquake focal mechanisms, moment tensors, and the consistency of seismic activity near plate boundaries. *Tectonics* **1992**, *11*, 279–296. [[CrossRef](#)]
55. Baraza, J.; Ercilla, G.; Nelson, C.H. Potential geologic hazards on the eastern Gulf of Cadiz slope (SW Spain). *Mar. Geol.* **1999**, *155*, 191–215. [[CrossRef](#)]
56. Gahalaut, V.K.; Kundu, B.; Laishram, S.S.; Catherine, J.; Kumar, A.; Singh, M.D.; Tiwari, R.P.; Chadha, R.K.; Samanta, S.K.; Ambikapathy, A.; et al. Aseismic plate boundary in the Indo-Burmese wedge, Northwest Sunda Arc. *Geology* **2013**, *41*, 235–238. [[CrossRef](#)]
57. Avouac, J.-P. From geodetic imaging of seismic and aseismic fault slip to dynamic modeling of the seismic cycle. *Annu. Rev. Earth Planet. Sci.* **2015**, *43*, 233–271. [[CrossRef](#)]
58. Wang, K.; Hu, Y.; He, J. Deformation cycles of subduction earthquakes in a viscoelastic earth. *Nature* **2012**, *484*, 327–332. [[CrossRef](#)]
59. Cloos, M. Thrust-type subduction-zone earthquakes and seamount asperities: A physical model for seismic rupture. *Geology* **1992**, *20*, 601–604. [[CrossRef](#)]
60. Polet, J.; Kanamori, H. Shallow subduction zone earthquakes and their tsunamigenic potential. *Geophys. J. Int.* **2000**, *142*, 684–702. [[CrossRef](#)]
61. Kaneda, Y.; Kawaguchi, K.; Araki, E.; Matsumoto, H.; Nakamura, T.; Kamiya, S.; Ariyoshi, K.; Hori, T.; Baba, T.; Takahashi, N. Development and Application of an Advanced Ocean Floor Network System for Megathrust Earthquakes and Tsunamis. In *Seafloor Observatories: A New Vision of the Earth from the Abyss*; Favali, P., Beranzoli, L., De Santis, A., Eds.; Springer: Berlin/Heidelberg, Germany, 2015; pp. 643–662.
62. Tajima, F.; Mori, J.; Kennett, B.L.N. A review of the 2011 Tohoku-Oki earthquake (Mw 9.0): Large-scale rupture across heterogeneous plate coupling. *Tectonophysics* **2013**, *586*, 15–34. [[CrossRef](#)]
63. Choy, G.L.; McGarr, A. Strike-slip earthquakes in the oceanic lithosphere: Observations of exceptionally high apparent stress. *Geophys. J. Int.* **2002**, *150*, 506–523. [[CrossRef](#)]
64. Tanioka, Y.; Satake, K. Tsunami generation by horizontal displacement of ocean bottom. *Geophys. Res. Lett.* **1996**, *23*, 861–864. [[CrossRef](#)]
65. Galindo-Zaldívar, J.; Jabaloy, A.; Maldonado, A.; Martínez-Martínez, J.M.; de Galdeano, C.S.; Somoza, L.; Surinach, E. Deep crustal structure of the area of intersection between the Shackleton fracture zone and the West Scotia Ridge (Drake Passage, Antarctica). *Tectonophysics* **2000**, *320*, 123–139. [[CrossRef](#)]
66. Maldonado, A.; Balanyá, J.C.; Barnolas, A.; Galindo-Zaldívar, J.; Hernández, J.; Jabaloy, A.; Livermore, R.; Martínez, J.M.; Rodríguez-Fernández, J.; de Galdeano, C.S.; et al. Tectonics of an extinct ridge-transform intersection, Drake Passage (Antarctica). *Mar. Geophys. Res.* **2000**, *21*, 43–68. [[CrossRef](#)]
67. Estrada, F.; González-Vida, J.M.; Peláez, J.A.; Galindo-Zaldívar, J.; Ercilla, G.; Vázquez, J.T. Tsunamigenic Risk Associated to Vertical Offset in Transcurrent Fault Termination: The Case of the Averroes Fault (Alboran Sea). In *Proceedings of the Fault2SHA—4th Workshop, Barcelona, Spain, 3–5 June 2019*; ICM-CSIC: Barcelona, Spain, 2019; pp. 14–15.
68. Pisarska-Jamroz, M.; Belzyt, S.; Börner, A.; Hoffmann, G.; Hüneke, H.; Kenzler, M.; Obst, K.; Rother, H.; van Loon, A.J. Evidence from seismites for glacio-isostatically induced crustal faulting in front of an advancing land-ice mass (Rügen island, SW Baltic sea). *Tectonophysics* **2018**, *745*, 338–348. [[CrossRef](#)]

69. Goldfinger, C.; Nelson, C.H.; Morey, A.E.; Johnson, J.E.; Patton, J.R.; Karabanov, E.; Gutiérrez-Pastor, J.; Eriksson, A.T.; Gràcia, E.; Dunhill, G.; et al. *Turbidite Event History—Methods and Implications for Holocene Paleoseismicity of the Cascadia Subduction Zone*; U.S. Geological Survey: Reston, VA, USA, 2012.
70. Masson, D.G.; Kenyon, N.H.; Weaver, P.P.E. Slides, debris Flows, and Turbidity Currents. In *Oceanography: An Illustrated Guide*; Summerhayes, C.P., Thorpe, S.A., Eds.; Manson Publishing: London, UK, 1996; pp. 136–151.
71. Nardin, T.R.; Hein, F.J.; Gorsline, D.S.; Edwards, B.D. A Review of Mass Movement Processes, Sediment and Acoustic Characteristics, and Contrasts in Slope and Base-Of-Slope Systems Versus Canyon-Fan-Basin Floor Systems. In *Geology of Continental Slopes*; Doyle, L.J., Pilkey, O.H., Eds.; SEPM Society for Sedimentary Geology: Tulsa, OK, USA, 1979; Volume 27, pp. 61–73.
72. Mulder, T.; Cochonat, P. Classification of offshore mass movements. *J. Sediment. Res.* **1996**, *66*, 43–57. [[CrossRef](#)]
73. Shanmugam, G. 50 years of the turbidite paradigm (1950s–1990s): Deep-water processes and facies models—A critical perspective. *Mar. Pet. Geol.* **2000**, *17*, 285–342. [[CrossRef](#)]
74. Tripsanas, E.K.; Piper, D.J.; Jenner, K.A.; Bryant, W.R. Submarine mass-transport facies: New perspectives on flow processes from cores on the eastern North American margin. *Sedimentology* **2008**, *55*, 97–136. [[CrossRef](#)]
75. Frey-Martínez, J.; Cartwright, J.; James, D. Frontally confined versus frontally emergent submarine landslides: A 3D seismic characterisation. *Mar. Pet. Geol.* **2006**, *23*, 585–604. [[CrossRef](#)]
76. Moscardelli, L.; Wood, L. New classification system for mass transport complexes in offshore Trinidad. *Basin Res.* **2008**, *20*, 73–98. [[CrossRef](#)]
77. Canals, M.; Puig, P.; de Madron, X.D.; Heussner, S.; Palanques, A.; Fabres, J. Flushing submarine canyons. *Nature* **2006**, *444*, 354–357. [[CrossRef](#)] [[PubMed](#)]
78. Talling, P.J.; Paull, C.K.; Piper, D.J.W. How are subaqueous sediment density flows triggered, what is their internal structure and how does it evolve? Direct observations from monitoring of active flows. *Earth Sci. Rev.* **2013**, *125*, 244–287. [[CrossRef](#)]
79. Clare, M.A.; Vardy, M.E.; Cartigny, M.J.; Talling, P.J.; Himsforth, M.D.; Dix, K.; Harris, J.M.; Whitehouse, R.J.S.; Belal, M. Direct monitoring of active geohazards: Emerging geophysical tools for deep-water assessments. *Near Surf. Geophys.* **2017**, *15*, 427–444. [[CrossRef](#)]
80. Gwiazda, R.; Paull, C.K.; Ussler, W.; Alexander, C.R. Evidence of modern fine-grained sediment accumulation in the Monterey fan from measurements of the pesticide DDT and its metabolites. *Mar. Geol.* **2015**, *363*, 125–133. [[CrossRef](#)]
81. Azpiroz-Zabala, M.; Cartigny, M.J.B.; Talling, P.J.; Parsons, D.R.; Sumner, E.J.; Clare, M.A.; Simmons, S.M.; Cooper, C.; Pope, E.L. Newly recognized turbidity current structure can explain prolonged flushing of submarine canyons. *Sci. Adv.* **2017**, *3*, e1700200. [[CrossRef](#)]
82. Locat, J.; Leroueil, S.; Locat, A.; Lee, H. Weak Layers: Their Definition and Classification from a Geotechnical Perspective. In *Submarine Mass Movements and their Consequences*; Krastel, S., Behrmann, J.-H., Völker, D., Stipp, M., Berndt, C., Urgeles, R., Chaytor, J., Huhn, K., Strasser, M., Harbitz, C.B., Eds.; Springer: Cham, Switzerland, 2014; pp. 3–12.
83. Hutchinson, J. General Report: Morphological and Geotechnical Parameters of Landslides in Relation to Geology and Hydrogeology. In Proceedings of the 5th International Symposium on Landslides, Lausanne, Switzerland, 10–15 July 1988; Bonnard, C., Ed.; August Aimé Balkema: Rotterdam, The Netherlands, 1988; Volume 5, pp. 3–35.
84. Mulder, T.; Alexander, J. The physical character of subaqueous sedimentary density flows and their deposits. *Sedimentology* **2001**, *48*, 269–299. [[CrossRef](#)]
85. Masson, D.G.; Watts, A.B.; Gee, M.J.R.; Urgeles, R.; Mitchell, N.C.; Le Bas, T.P.; Canals, M. Slope failures on the flanks of the western Canary islands. *Earth Sci. Rev.* **2002**, *57*, 1–35. [[CrossRef](#)]
86. Normark, W.R.; Piper, D.J.W. Initiation Processes and Flow Evolution of Turbidity Currents: Implications for the Depositional Record. In *From Shoreline to Abyss: Contributions in Marine Geology in Honor of Francis Parker Shepard*; Osborne, R.H., Ed.; SEPM Society for Sedimentary Geology: Tulsa, OK, USA, 1991; Volume 46, pp. 207–230.
87. Casas, D.; Ercilla, G.; García, M.; Yenes, M.; Estrada, F. Post-rift sedimentary evolution of the Gebra Debris Valley. A submarine slope failure system in the Central Bransfield basin (Antarctica). *Mar. Geol.* **2013**, *340*, 16–29. [[CrossRef](#)]
88. Casas, D.; García, M.; Bohoyo, F.; Maldonado, A.; Ercilla, G. The Gebra–Magia complex: Mass-transport processes reworking trough-mouth fans in the Central Bransfield basin (Antarctica). *Geol. Soc. Lond. Spec. Publ.* **2018**, *461*, 61–75. [[CrossRef](#)]
89. De Blasio, F.V. Dynamics of Mass Flows and of Sediment Transport in Amazonis Planitia, Mars. In Proceedings of the European Planetary Science Congress 2013, London, UK, 8–13 September 2013; EPSC: London, UK, 2013; Volume 8, pp. 1–2.
90. Urlaub, M.; Talling, P.; Zervos, A. A Numerical Investigation of Sediment Destructuring as a Potential Globally Widespread Trigger for Large Submarine Landslides on Low Gradients. In *Submarine Mass Movements and their Consequences*; Krastel, S., Behrmann, J.-H., Völker, D., Stipp, M., Berndt, C., Urgeles, R., Chaytor, J., Huhn, K., Strasser, M., Harbitz, C.B., Eds.; Springer: Cham, Switzerland, 2014; pp. 177–188.
91. Stevenson, C.J.; Jackson, C.A.L.; Hodgson, D.M.; Hubbard, S.M.; Eggenhuisen, J.T. Deep-water sediment bypass. *J. Sediment. Res.* **2015**, *85*, 1058–1081. [[CrossRef](#)]
92. Hizzett, J.L.; Clarke, J.E.H.; Sumner, E.J.; Cartigny, M.J.B.; Talling, P.J.; Clare, M.A. Which triggers produce the most erosive, frequent, and longest runout turbidity currents on deltas? *Geophys. Res. Lett.* **2017**, *45*, 855–863. [[CrossRef](#)]
93. Paull, C.K.; Talling, P.J.; Maier, K.L.; Parsons, D.; Xu, J.; Caress, D.W.; Gwiazda, R.; Lundsten, E.M.; Anderson, K.; Barry, J.P.; et al. Powerful turbidity currents driven by dense basal layers. *Nat. Commun.* **2018**, *9*, 4114. [[CrossRef](#)] [[PubMed](#)]

94. Miramontes, E.; Eggenhuisen, J.T.; Jacinto, R.S.; Poneti, G.; Pohl, F.; Normandeau, A.; Campbell, D.C.; Hernández-Molina, F.J. Channel-levee evolution in combined contour current-turbidity current flows from flume tank experiments. *Geology* **2020**, *48*, 353–357. [[CrossRef](#)]
95. Guzzetti, F.; Malamud, B.D.; Turcotte, D.L.; Reichenbach, P. Power-law correlations of landslide areas in central Italy. *Earth Planet. Sci. Lett.* **2002**, *195*, 169–183. [[CrossRef](#)]
96. Thomas, S.; Hooper, J.; Clare, M. Constraining Geohazards to the Past: Impact Assessment of Submarine Mass Movements on Seabed Developments. In *Submarine Mass Movements and Their Consequences*; Mosher, D.C., Shipp, R.C., Moscardelli, L., Chaytor, J.D., Baxter, C.D.P., Lee, H.J., Urgeles, R., Eds.; Springer: Dordrecht, The Netherlands, 2010; pp. 387–398.
97. Casas, D.; Chiocci, F.; Casalbore, D.; Ercilla, G.; de Urbina, J.O. Magnitude-frequency distribution of submarine landslides in the Gioia basin (Southern Tyrrhenian sea). *Geo-Mar. Lett.* **2016**, *36*, 405–414. [[CrossRef](#)]
98. Stark, C.P.; Hovius, N. The characterization of landslide size distributions. *Geophys. Res. Lett.* **2001**, *28*, 1091–1094. [[CrossRef](#)]
99. Di Traglia, F.; Nolesini, T.; Solari, L.; Ciampalini, A.; Frodella, W.; Steri, D.; Allotta, B.; Rindi, A.; Marini, L.; Monni, N.; et al. Lava delta deformation as a proxy for submarine slope instability. *Earth Planet. Sci. Lett.* **2018**, *488*, 46–58. [[CrossRef](#)]
100. Trofimovs, J.; Amy, L.; Boudon, G.; Deplus, C.; Doyle, E.; Fournier, N.; Hart, M.B.; Komorowski, J.C.; Le Friant, A.; Lock, E.J.; et al. Submarine pyroclastic deposits formed at the Soufrière Hills volcano, Montserrat (1995–2003): What happens when pyroclastic flows enter the ocean? *Geology* **2006**, *34*, 549–552. [[CrossRef](#)]
101. Casalbore, D.; Clementucci, R.; Bosman, A.; Chiocci, F.L.; Martorelli, E.; Ridente, D. Widespread mass-wasting processes off NE Sicily (Italy): Insights from morpho-bathymetric analysis. *Geol. Soc. Lond. Spec. Publ.* **2020**, *500*, 393–403. [[CrossRef](#)]
102. Kokelaar, P. Magma-water interactions in subaqueous and emergent basaltic. *Bull. Volcanol.* **1986**, *48*, 275–289. [[CrossRef](#)]
103. Kueppers, U.; Nichols, A.R.L.; Zanon, V.; Potuzak, M.; Pacheco, J.M.R. Lava balloons—Peculiar products of basaltic submarine eruptions. *Bull. Volcanol.* **2012**, *74*, 1379–1393. [[CrossRef](#)]
104. Perfit, M.R.; Chadwick, W.W. Magmatism at mid-ocean ridges: Constraints from volcanological and geochemical investigations. *Geophys. Monogr. Am. Geophys. Union* **1998**, *106*, 59–116. [[CrossRef](#)]
105. McClinton, J.T.; White, S.M.; Colman, A.; Rubin, K.H.; Sinton, J.M. The role of crystallinity and viscosity in the formation of submarine lava flow morphology. *Bull. Volcanol.* **2014**, *76*, 854. [[CrossRef](#)]
106. Jutzeler, M.; Marsh, R.; Carey, R.J.; White, J.D.L.; Talling, P.J.; Karlstrom, L. On the fate of pumice rafts formed during the 2012 havre submarine eruption. *Nat. Commun.* **2014**, *5*, 3660. [[CrossRef](#)]
107. Bosman, A.; Casalbore, D.; Romagnoli, C.; Chiocci, F.L. Formation of an ‘a’ā lava delta: Insights from time-lapse multibeam bathymetry and direct observations during the stromboli 2007 eruption. *Bull. Volcanol.* **2014**, *76*, 838. [[CrossRef](#)]
108. Fraile-Nuez, E.; González-Dávila, M.; Santana-Casiano, J.M.; Arístegui, J.; Alonso-González, I.J.; Hernández-León, S.; Blanco, M.J.; Rodríguez-Santana, A.; Hernández-Guerra, A.; Gelado-Caballero, M.D.; et al. The submarine volcano eruption at the island of El Hierro: Physical-chemical perturbation and biological response. *Sci. Rep.* **2012**, *2*, 486. [[CrossRef](#)] [[PubMed](#)]
109. McClinton, J.T.; White, S.M. Emplacement of submarine lava flow fields: A geomorphological model from the niños eruption at the galápagos spreading center. *Geochem. Geophys. Geosystems* **2015**, *16*, 899–911. [[CrossRef](#)]
110. Santana-Casiano, J.M.; González-Dávila, M.; Fraile-Nuez, E.; de Armas, D.; González, A.G.; Domínguez-Yanes, J.F.; Escáñez, J. The natural ocean acidification and fertilization event caused by the submarine eruption of El Hierro. *Sci. Rep.* **2013**, *3*, 1140. [[CrossRef](#)]
111. White, J.D.L.; McPhie, J.; Soule, S.A. Submarine Lavas and Hyaloclastite. In *The Encyclopedia of Volcanoes*, 2nd ed.; Sigurdsson, H., Ed.; Academic Press: Amsterdam, The Netherlands, 2015; Chapter 19; pp. 363–375.
112. White, J.D.L.; Schipper, C.I.; Kano, K. Submarine Explosive Eruptions. In *The Encyclopedia of Volcanoes*, 2nd ed.; Sigurdsson, H., Ed.; Academic Press: Amsterdam, The Netherlands, 2015; Chapter 31; pp. 553–569.
113. Casalbore, D. Volcanic Islands and Seamounts. In *Submarine Geomorphology*; Micallef, A., Krastel, S., Savini, A., Eds.; Springer: Cham, Switzerland, 2018; pp. 333–347.
114. Cas, R.A.F.; Giordano, G. Submarine volcanism: A review of the constraints, processes and products, and relevance to the cabo de gata volcanic succession. *Ital. J. Geosci.* **2014**, *133*, 362–377. [[CrossRef](#)]
115. Rivera, J.; Lastras, G.; Canals, M.; Acosta, J.; Arrese, B.; Hermida, N.; Micallef, A.; Tello, O.; Amblas, D. Construction of an oceanic island: Insights from the El Hierro (Canary islands) 2011–2012 submarine volcanic eruption. *Geology* **2013**, *41*, 355–358. [[CrossRef](#)]
116. Embley, R.W.; Merle, S.G.; Baker, E.T.; Rubin, K.H.; Lupton, J.E.; Resing, J.A.; Dziak, R.P.; Lilley, M.D.; Chadwick, W.W.; Shank, T.; et al. Eruptive modes and hiatus of volcanism at West Mata seamount, NE Lau basin: 1996–2012. *Geochem. Geophys. Geosystems* **2014**, *15*, 4093–4115. [[CrossRef](#)]
117. Somoza, L.; González, F.J.; Barker, S.J.; Madureira, P.; Medialdea, T.; de Ignacio, C.; Lourenço, N.; León, R.; Vázquez, J.T.; Palomino, D. Evolution of submarine eruptive activity during the 2011–2012 El Hierro event as documented by hydroacoustic images and remotely operated vehicle observations. *Geochem. Geophys. Geosyst.* **2017**, *18*, 3109–3137. [[CrossRef](#)]
118. Casas, D.; Pimentel, A.; Pacheco, J.; Martorelli, E.; Sposato, A.; Ercilla, G.; Alonso, B.; Chiocci, F. Serreta 1998–2001 submarine volcanic eruption, offshore Terceira (Azores): Characterization of the vent and inferences about the eruptive dynamics. *J. Volcanol. Geotherm. Res.* **2018**, *356*, 127–140. [[CrossRef](#)]
119. Tepp, G.; Chadwick, W.W.; Haney, M.M.; Lyons, J.J.; Dziak, R.P.; Merle, S.G.; Butterfield, D.A.; Young, C.W. Hydroacoustic, seismic, and bathymetric observations of the 2014 submarine eruption at Ahyi seamount, Mariana Arc. *Geochem. Geophys. Geosystems* **2019**, *20*, 3608–3627. [[CrossRef](#)]

120. Le Saout, M.; Bohnenstiehl, D.R.; Paduan, J.B.; Clague, D.A. Quantification of eruption dynamics on the north rift at Axial seamount, Juan de Fuca Ridge. *Geochem. Geophys. Geosystems* **2020**, *21*, e2020GC009136. [CrossRef]
121. Kelley, D.S.; Delaney, J.R.; Juniper, S.K. Establishing a new era of submarine volcanic observatories: Cabling Axial seamount and the endeavour segment of the Juan de Fuca Ridge. *Mar. Geol.* **2014**, *352*, 426–450. [CrossRef]
122. Judd, A.; Hovland, M. *Seabed Fluid Flow: The Impact on Geology, Biology and the Marine Environment*; Cambridge University Press: Cambridge, UK, 2007.
123. Martínez-Carreño, N.; García-Gil, S. The holocene gas system of the Ría de Vigo (NW Spain): Factors controlling the location of gas accumulations, seeps and pockmarks. *Mar. Geol.* **2013**, *344*, 82–100. [CrossRef]
124. García-Gil, S.; Cartelle, V.; de Blas, E.; de Carlos, A.R.; Díez, R.; Durán, R.; Ferrín, A.; García-Moreiras, I.; García-García, A.; Iglesias, J.; et al. Gas somero en el margen continental Ibérico. *Bol. Geol. Min.* **2015**, *126*, 575–608.
125. Cartwright, J. The impact of 3D seismic data on the understanding of compaction, fluid flow and diagenesis in sedimentary basins. *J. Geol. Soc.* **2007**, *164*, 881–893. [CrossRef]
126. Sun, Q.; Wu, S.; Cartwright, J.; Dong, D. Shallow gas and focused fluid flow systems in the Pearl river mouth basin, Northern South China sea. *Mar. Geol.* **2012**, *315–318*, 1–14. [CrossRef]
127. Andreassen, K.; Hubbard, A.; Winsborrow, M.; Patton, H.; Vadakkepuliambatta, S.; Plaza-Faverola, A.; Gudlaugsson, E.; Serov, P.; Deryabin, A.; Mattingsdal, R.; et al. Massive blow-out craters formed by hydrate-controlled methane expulsion from the Arctic seafloor. *Science* **2017**, *356*, 948–953. [CrossRef]
128. BOEM. *Gulf of Mexico Deepwater Bathymetry with Hillshade*; Bureau of Ocean Energy Management: Washington, DC, USA, 2016.
129. BOEM. *BOEM Seismic Water Bottom Anomalies—Gulf of Mexico—Gulf of Mexico NAD27*; Bureau of Ocean Energy Management: Washington, DC, USA, 2016.
130. Milkov, A.V. Global Distribution of Mud Volcanoes and Their Significance in Petroleum Exploration as a Source of Methane in the Atmosphere and Hydrosphere and as a Geohazard. In *Mud Volcanoes, Geodynamics and Seismicity*; Martinelli, G., Panahi, B., Eds.; Springer: Dordrecht, The Netherlands, 2005; pp. 29–34.
131. Etiope, G.; Klusman, R.W. Geologic emissions of methane to the atmosphere. *Chemosphere* **2002**, *49*, 777–789. [CrossRef]
132. Ciais, P.; Chris, S.; Govindasamy, B.; Bopp, L.; Brovkin, V.; Canadell, J.; Chhabra, A.; Defries, R.; Galloway, J.; Heimann, M. Carbon and Other Biogeochemical Cycles. In *Climate Change 2013: The Physical Science Basis*; Stocker, T.F., Ed.; Cambridge University Press: Cambridge, UK, 2013; pp. 465–570.
133. Etiope, G. *Natural Gas Seepage: The Earth's Hydrocarbon Degassing*; Springer: Cham, Switzerland, 2015.
134. Fernández-Puga, M.C.; Vázquez, J.T.; Somoza, L.; del Río, V.D.; Medialdea, T.; Mata, M.P.; León, R. Gas-related morphologies and diapirism in the Gulf of Cádiz. *Geo-Mar. Lett.* **2007**, *27*, 213–221. [CrossRef]
135. Eiby, G.A. Earthquakes and tsunamis in a region of diapiric folding. *Tectonophysics* **1982**, *85*, T1–T8. [CrossRef]
136. Kvenvolden, K.A. A primer on the geological occurrence of gas hydrate. *Geol. Soc. Lond. Spec. Publ.* **1998**, *137*, 9–30. [CrossRef]
137. Soloviev, V.; Ginsburg, G.D. Formation of submarine gas hydrates. *Bull. Geol. Soc. Den.* **1994**, *41*, 86–94.
138. Hesse, R. Pore water anomalies of submarine gas-hydrate zones as tool to assess hydrate abundance and distribution in the subsurface what have we learned in the past decade? *Earth Sci. Rev.* **2003**, *61*, 149–179. [CrossRef]
139. Cunningham, R.; Lindholm, R. Seismic Evidence for Widespread Gas Hydrate Formation, Offshore West Africa. In *Petroleum Systems of South Atlantic Margins*; AAPG: Tulsa, OK, USA, 2000; pp. 93–105. [CrossRef]
140. IUSGS. Gas Hydrates-Primer. Available online: <https://www.usgs.gov/centers/whcmssc/science/gas-hydrates-primer> (accessed on 12 November 2020).
141. Nixon, M.F.; Grozic, J.L. Submarine slope failure due to gas hydrate dissociation: A preliminary quantification. *Can. Geotech. J.* **2007**, *44*, 314–325. [CrossRef]
142. Shanmugam, G. *New Perspectives on Deep-Water Sandstones: Origin, Recognition, Initiation, and Reservoir Quality*; Elsevier: Amsterdam, The Netherlands, 2012.
143. Mienert, J.; Vanneste, M.; Bünz, S.; Andreassen, K.; Haflidason, H.; Sejrup, H.P. Ocean warming and gas hydrate stability on the Mid-Norwegian margin at the storegga slide. *Mar. Pet. Geol.* **2005**, *22*, 233–244. [CrossRef]
144. Meinert, J. *Methane Hydrate and Submarine Slides*; Elsevier: Amsterdam, The Netherlands, 2009.
145. Elger, J.; Berndt, C.; Rüpke, L.; Krastel, S.; Gross, F.; Geissler, W.H. Submarine slope failures due to pipe structure formation. *Nat. Commun.* **2018**, *9*, 715. [CrossRef] [PubMed]
146. Judd, A.G.; Hovland, M.; Dimitrov, L.I.; Gil, S.G.; Jukes, V. The geological methane budget at continental margins and its influence on climate change. *Geofluids* **2002**, *2*, 109–126. [CrossRef]
147. Garcia-Gil, S.; Vilas, F.; Garcia-Garcia, A. Shallow gas features in incised-valley fills (Ría de Vigo, NW Spain): A case study. *Cont. Shelf Res.* **2002**, *22*, 2303–2315. [CrossRef]
148. Garcia-Gil, S. A natural laboratory for shallow gas: The Ras Baixas (NW Spain). *Geo-Mar. Lett.* **2003**, *23*, 215–229. [CrossRef]
149. Sharke, A.; Ruppel, C.; Kodis, M.; Brothers, D.; Lobecker, E. Widespread methane leakage from the sea floor on the Northern US Atlantic margin. *Nat. Geosci.* **2014**, *7*, 657–661. [CrossRef]
150. Rebesco, M.; Camerlenghi, A.; Van Loon, A.J. Contourite research: A field in full development. *Dev. Sedimentol.* **2008**, *60*, 1–10. [CrossRef]
151. Stow, D.A.V.; Hernández-Molina, F.J.; Llave, E.; Sayago-Gil, M.; del Río, V.D.; Branson, A. Bedform-velocity matrix: The estimation of bottom current velocity from bedform observations. *Geology* **2009**, *37*, 327–330. [CrossRef]

152. Hollister, C.D.; Heezen, B.C. Geological Effects of Ocean Bottom Currents: Western North Atlantic. In *Studies in Physical Oceanography*; Gordon, A.L., Ed.; Gordon and Breach: New York, NY, USA, 1972; Volume 2, pp. 37–66.
153. Llave, E.; Schönfeld, J.; Hernández-Molina, F.J.; Mulder, T.; Somoza, L.; del Río, V.D.; Sánchez-Almazo, I. High-resolution stratigraphy of the Mediterranean outflow contourite system in the Gulf of Cadiz during the late pleistocene: The impact of Heinrich events. *Mar. Geol.* **2006**, *227*, 241–262. [[CrossRef](#)]
154. Kaboth, S.; de Boer, B.; Bahr, A.; Zeeden, C.; Lourens, L.J. Mediterranean outflow water dynamics during the past ~570 kyr: Regional and global implications. *Paleoceanography* **2017**, *32*, 634–647. [[CrossRef](#)]
155. Rebesco, M.; Hernández-Molina, F.J.; Van Rooij, D.; Wåhlin, A. Contourites and associated sediments controlled by deep-water circulation processes: State-of-the-art and future considerations. *Mar. Geol.* **2014**, *352*, 111–154. [[CrossRef](#)]
156. Hernández-Molina, F.J.; Wåhlin, A.; Bruno, M.; Ercilla, G.; Llave, E.; Serra, N.; Rosón, G.; Puig, P.; Rebesco, M.; Van Rooij, D.; et al. Oceanographic processes and morphosedimentary products along the Iberian margins: A new multidisciplinary approach. *Mar. Geol.* **2016**, *378*, 127–156. [[CrossRef](#)]
157. Ercilla, G.; Casas, D.; Hernández-Molina, F.J.; Roque, C. Generation of Bedforms by the Mediterranean Outflow Current at the Exit of the Strait of Gibraltar. In *Atlas of Bedforms in the Western Mediterranean*; Guillén, J., Acosta-Yepes, J., Chiocci, F.L., Palanques, A., Eds.; Springer: Cham, Switzerland, 2017; pp. 273–280.
158. Teixeira, M.; Terrinha, P.; Roque, C.; Rosa, M.; Ercilla, G.; Casas, D. Interaction of alongslope and downslope processes in the Alentejo Margin (SW Iberia)—Implications on slope stability. *Mar. Geol.* **2019**, *410*, 88–108. [[CrossRef](#)]
159. Kuijpers, A.; Nielsen, T. Near-bottom current speed maxima in North Atlantic contourite environments inferred from current-induced bedforms and other seabed evidence. *Mar. Geol.* **2016**, *378*, 230–236. [[CrossRef](#)]
160. Hernández-Molina, F.J.; Llave, E.; Stow, D.A.V.; García, M.; Somoza, L.; Vázquez, J.T.; Lobo, F.J.; Maestro, A.; del Río, V.D.; León, R.; et al. The contourite depositional system of the Gulf of Cádiz: A sedimentary model related to the bottom current activity of the Mediterranean outflow water and its interaction with the continental margin. *Deep Sea Res. Part II Top. Stud. Oceanogr.* **2006**, *53*, 1420–1463. [[CrossRef](#)]
161. Martorelli, E.; Bosman, A.; Casalbore, D.; Falcini, F. Interaction of down-slope and along-slope processes off Capo Vaticano (southern Tyrrhenian sea, Italy), with particular reference to contourite-related landslides. *Mar. Geol.* **2016**, *378*, 43–55. [[CrossRef](#)]
162. Ercilla, G.; Juan, C.; Hernández-Molina, F.J.; Bruno, M.; Estrada, F.; Alonso, B.; Casas, D.; Farran, M.I.; Llave, E.; García, M.; et al. Significance of bottom currents in deep-sea morphodynamics: An example from the Alboran sea. *Mar. Geol.* **2016**, *378*, 157–170. [[CrossRef](#)]
163. Juan, C.; Ercilla, G.; Estrada, F.; Alonso, B.; Casas, D.; Vázquez, J.T.; d’Acremont, E.; Medialdea, T.; Hernández-Molina, F.J.; Gorini, C.; et al. Multiple factors controlling the deep marine sedimentation of the Alboran sea (SW Mediterranean) after the Zanclean Atlantic mega-flood. *Mar. Geol.* **2020**, *423*, 106138. [[CrossRef](#)]
164. Casas, D.; Yenes, M.; Urgeles, R. Submarine mass movements around the Iberian Peninsula. The building of continental margins through hazardous processes. *Bol. Geol. Min.* **2015**, *126*, 257–278.
165. Droghei, R.; Falcini, F.; Casalbore, D.; Martorelli, E.; Mosetti, R.; Sannino, G.; Santoleri, R.; Chiocci, F.L. The role of internal solitary waves on deep-water sedimentary processes: The case of up-slope migrating sediment waves off the Messina strait. *Sci. Rep.* **2016**, *6*, 36376. [[CrossRef](#)]
166. Palomino, D.; Vázquez, J.T.; Ercilla, G.; Alonso, B.; López-González, N.; Díaz-del-Río, V. Interaction between seabed morphology and water masses around the seamounts on the Motril Marginal Plateau (Alboran sea, Western Mediterranean). *Geo-Mar. Lett.* **2011**, *31*, 465–479. [[CrossRef](#)]
167. Falcini, F.; Martorelli, E.; Chiocci, F.L.; Salusti, E. A general theory for the effect of local topographic unevenness on contourite deposition around marine capes: An inverse problem applied to the Italian continental margin (Cape Suvero). *Mar. Geol.* **2016**, *378*, 74–80. [[CrossRef](#)]
168. Miramontes, E.; Garreau, P.; Caillaud, M.; Jouet, G.; Pellen, R.; Hernández-Molina, F.J.; Clare, M.A.; Cattaneo, A. Contourite distribution and bottom currents in the NW Mediterranean sea: Coupling seafloor geomorphology and hydrodynamic modelling. *Geomorphology* **2019**, *333*, 43–60. [[CrossRef](#)]
169. Puig, P.; Palanques, A.; Guillén, J.; El Khatib, M. Role of internal waves in the generation of nepheloid layers on the Northwestern Alboran slope: Implications for continental margin shaping. *J. Geophys. Res.* **2004**, *109*, C09011. [[CrossRef](#)]
170. Séranne, M.; Abeigne, C.R.N. Oligocene to holocene sediment drifts and bottom currents on the slope of Gabon continental margin (West Africa): Consequences for sedimentation and southeast Atlantic upwelling. *Sediment. Geol.* **1999**, *128*, 179–199. [[CrossRef](#)]
171. Sarhan, T. Upwelling mechanisms in the Northwestern Alboran sea. *J. Mar. Syst.* **2000**, *23*, 317–331. [[CrossRef](#)]
172. Macias, D.; Garcia-Gorriz, E.; Stips, A. The seasonal cycle of the Atlantic jet dynamics in the Alboran sea: Direct atmospheric forcing versus Mediterranean thermohaline circulation. *Ocean Dyn.* **2016**, *66*, 137–151. [[CrossRef](#)]
173. Fogliani, F.; Campiani, E.; Trincardi, F. The reshaping of the South West Adriatic margin by cascading of dense shelf waters. *Mar. Geol.* **2016**, *375*, 64–81. [[CrossRef](#)]
174. Ercilla, G.; Casas, D.; Estrada, F.; Vázquez, J.T.; Iglesias, J.; García, M.; Gómez, M.; Acosta, J.; Gallart, J.; Maestro-González, A. Morphosedimentary features and recent depositional architectural model of the Cantabrian continental margin. *Mar. Geol.* **2008**, *247*, 61–83. [[CrossRef](#)]

175. Juan, C.; Ercilla, G.; Hernández-Molina, F.J.; Estrada, F.; Alonso, B.; Casas, D.; García, M.; Farran, M.L.; Llave, E.; Palomino, D.; et al. Seismic evidence of current-controlled sedimentation in the Alboran sea during the pliocene and quaternary: Palaeoceanographic implications. *Mar. Geol.* **2016**, *378*, 292–311. [[CrossRef](#)]
176. Laberg, J.S.; Baeten, N.J.; Vanneste, M.; Forsberg, C.F.; Forwick, M.; Haflidason, H. Sediment Failure Affecting Muddy Contourites on the Continental Slope Offshore Northern Norway: Lessons Learned and Some Outstanding Issues. In *Submarine Mass Movements and their Consequences*; Lamarche, G., Mountjoy, J., Eds.; Springer: Cham, Switzerland, 2016; pp. 281–289.
177. Ercilla, G.; Galindo-Zaldívar, J.; Valencia, J.; Tendero-Salmeron, V.; Estrada, F.; Casas, D.; Alonso, B.; d’Acremont, E.; Comas, M.; Tomas Vazquez, J.; et al. Understanding the Geomorphology of the Gulf of Vera (Western Mediterranean): Clues from Offshore and Onland Structures. In *EGU General Assembly Conference Abstracts*; EGU: Munich, Germany, 2019; Volume 21, p. 13411.
178. Röbbke, B.R.; Vött, A. The tsunami phenomenon. *Prog. Oceanogr.* **2017**, *159*, 296–322. [[CrossRef](#)]
179. Assier-Rzadkiewic, S.; Heinrich, P.; Sabatier, P.C.; Savoye, B.; Bourillet, J.F. Numerical modelling of a landslide-generated tsunami: The 1979 nice event. *Pure Appl. Geophys.* **2000**, *157*, 1707–1727. [[CrossRef](#)]
180. Geist, E.L. Local Tsunamis and Earthquake Source Parameters. In *Advances in Geophysics*; Dmowska, R., Saltzman, B., Eds.; Elsevier: Amsterdam, The Netherlands, 1997; Volume 39, pp. 117–209.
181. Bryant, E.A. *Tsunami: The Underrated Hazard*; Springer: Berlin/Heidelberg, Germany, 2014.
182. Tappin, D.R. Mass Transport Events and Their Tsunami Hazard. In *Submarine Mass Movements and their Consequences*; Mosher, D.C., Shipp, R.C., Moscardelli, L., Chaytor, J.D., Baxter, C.D.P., Lee, H.J., Urgeles, R., Eds.; Springer: Dordrecht, The Netherlands, 2010; pp. 667–684.
183. Tappin, D.R. Tsunamis from submarine landslides. *Geol. Today* **2017**, *33*, 190–200. [[CrossRef](#)]
184. González-Vida, J.M.; Macías, J.; Castro, M.J.; Sánchez-Linares, C.; de la Asunción, M.; Ortega-Acosta, S.; Arcas, D. The Lituya bay landslide-generated mega-tsunami—Numerical simulation and sensitivity analysis. *Nat. Hazards Earth Syst. Sci.* **2019**, *19*, 369–388. [[CrossRef](#)]
185. Løvholt, F.; Pedersen, G.; Harbitz, C.B.; Glimsdal, S.; Kim, J. On the characteristics of landslide tsunamis. *Philos. Trans. R. Soc. A Math. Phys. Eng. Sci.* **2015**, *373*, 20140376. [[CrossRef](#)]
186. Moore, J.G.; Normark, W.R.; Holcomb, R.T. Giant Hawaiian landslides. *Annu. Rev. Earth Planet. Sci.* **1994**, *22*, 119–144. [[CrossRef](#)]
187. Masson, D.G. Catastrophic collapse of the volcanic island of Hierro 15 ka ago and the history of landslides in the Canary islands. *Geology* **1996**, *24*, 231–234. [[CrossRef](#)]
188. Keating, B.H.; McGuire, W.J. Island edifice failures and associated tsunami hazards. *Pure Appl. Geophys.* **2000**, *157*, 899–955. [[CrossRef](#)]
189. Ayala-Carcedo, F.J.; Olcina Cantos, J. *Riesgos Naturales*; Editorial Ariel: Barcelona, Spain, 2002.
190. Levin, B.W.; Nosov, M.A. *Physics of Tsunamis*; Springer: Berlin/Heidelberg, Germany, 2016.
191. Macías, J.; Vázquez, J.T.; Fernández-Salas, L.M.; González-Vida, J.M.; Bárcenas, P.; Castro, M.J.; Díaz-del-Río, V.; Alonso, B. The Al-Borani submarine landslide and associated tsunami. A modelling approach. *Mar. Geol.* **2015**, *361*, 79–95. [[CrossRef](#)]
192. Pattiaratchi, C. Influence of ocean topography on tsunami propagation in Western Australia. *J. Mar. Sci. Eng.* **2020**, *8*, 629. [[CrossRef](#)]
193. Lu, C.Y.; Malavieille, J. Oblique convergence, indentation and rotation tectonics in the Taiwan mountain belt: Insights from experimental modelling. *Earth Planet. Sci. Lett.* **1994**, *121*, 477–494. [[CrossRef](#)]
194. Jiabiao, L.; Xianglong, J.; Aiguo, R.; Shimin, W.; Ziyin, W.; Jianhua, L. Indentation tectonics in the accretionary wedge of middle Manila Trench. *Chin. Sci. Bull.* **2004**, *49*, 1279–1288. [[CrossRef](#)]
195. Estrada, F.; Galindo-Zaldívar, J.; Vázquez, J.T.; Ercilla, G.; d’Acremont, E.; Alonso, B.; Gorini, C. Tectonic indentation in the Central Alboran sea (Westernmost Mediterranean). *Terra Nova* **2018**, *30*, 24–33. [[CrossRef](#)]
196. Coppier, G.; Griveaud, P.; de Larouziere, F.D.; Montenat, C.; d’Estevou, P.O. Example of neogene tectonic indentation in the eastern betic cordilleras: The Arc of Aguilas (Southeastern Spain). *Geodin. Acta* **1989**, *3*, 37–51. [[CrossRef](#)]
197. Cavalié, O.; Jónsson, S. Block-like plate movements in Eastern Anatolia observed by InSAR. *Geophys. Res. Lett.* **2014**, *41*, 26–31. [[CrossRef](#)]
198. Davy, P.; Cobbold, P. Indentation tectonics in nature and experiment. 1. Experiments scaled for gravity. *Bull. Geol. Inst. Univ. Upps.* **1988**, *14*, 129–141.
199. Lu, C.Y.; Chen, C.T.; Malavieille, J. Oblique Convergence, Indentation and Bivergent Tectonics in Taiwan: Insights from Field Observations and Analog Models. In *Geophysical Research Abstracts*; EGU: Munich, Germany, 2019; Volume 21.
200. Chiocci, F.L.; Ridente, D. Regional-scale seafloor mapping and geohazard assessment. The experience from the Italian project MaGIC (Marine Geohazards along the Italian Coasts). *Mar. Geophys. Res.* **2011**, *32*, 13–23. [[CrossRef](#)]
201. Iacono, C.L.; Sulli, A.; Agate, M.; Lo Presti, V.; Pepe, F.; Catalano, R. Submarine canyon morphologies in the Gulf of Palermo (Southern Tyrrhenian sea) and possible implications for geo-hazard. *Mar. Geophys. Res.* **2011**, *32*, 127–138. [[CrossRef](#)]
202. Huang, Z.; Nichol, S.L.; Harris, P.T.; Caley, M.J. Classification of submarine canyons of the Australian continental margin. *Mar. Geol.* **2014**, *357*, 362–383. [[CrossRef](#)]
203. Ercilla, G.; Juan, C.; Periañez, R.; Alonso, B.; Abril, J.M.; Estrada, F.; Casas, D.; Vázquez, J.T.; d’Acremont, E.; Gorini, C.; et al. Influence of alongslope processes on modern turbidite systems and canyons in the Alboran Sea (southwestern Mediterranean). *Deep Sea Res. I Oceanogr. Res. Pap.* **2019**, *144*, 1–16. [[CrossRef](#)]

204. Casas, D.; Ercilla, G.; Alonso, B.; Yenes, M.; Nespereira, J.; Estrada, F.; Ceramicola, S. Submarine Mass Movements Affecting the Almanzora-Alías-Garrucha Canyon System (SW Mediterranean)(SKT). In Proceedings of the 34th International Association of Sedimentologists (IAS) Meeting of Sedimentology, Sedimentology to Face Societal Challenges on Risk, Resources and Record of the Past, Rome, Italy, 10–13 September 2019.
205. Mazières, A.; Gillet, H.; Castelle, B.; Mulder, T.; Guyot, C.; Garlan, T.; Mallet, C. High-resolution morphobathymetric analysis and evolution of Capbreton submarine canyon head (Southeast bay of Biscay—French Atlantic Coast) over the last decade using descriptive and numerical modeling. *Mar. Geol.* **2014**, *351*, 1–12. [[CrossRef](#)]
206. Puig, P.; Palanques, A.; Martín, J. Contemporary sediment-transport processes in submarine canyons. *Annu. Rev. Mar. Sci.* **2014**, *6*, 53–77. [[CrossRef](#)] [[PubMed](#)]
207. Gómez-Ballesteros, M.; Druet, M.; Muñoz, A.; Arrese, B.; Rivera, J.; Sánchez, F.; Cristobo, J.; Parra, S.; García-Alegre, A.; González-Pola, C.; et al. Geomorphology of the avilés canyon system, Cantabrian sea (Bay of Biscay). *Deep Sea Res. II Top. Stud. Oceanogr.* **2014**, *106*, 99–117. [[CrossRef](#)]
208. Mountjoy, J.J.; Barnes, P.M.; Pettinga, J.R. Morphostructure and evolution of submarine canyons across an active margin: Cook Strait sector of the Hikurangi margin, New Zealand. *Mar. Geol.* **2009**, *260*, 45–68. [[CrossRef](#)]
209. Aranguiz, R.; Shibayama, T. Effect of submarine canyons on tsunami propagation: A case study of the biobio canyon, Chile. *Coast. Eng. J.* **2013**, *55*, 1350016–1–1350016–23. [[CrossRef](#)]
210. Casalbore, D.; Chiocci, F.L.; Mugnoz, G.S.; Tommasi, P.; Sposato, A. Flash-flood hyperpycnal flows generating shallow-water landslides at Fiumara mouths in Western Messina Strait (Italy). *Mar. Geophys. Res.* **2011**, *32*, 257–271. [[CrossRef](#)]
211. Micallef, A.; Mountjoy, J.J.; Barnes, P.M.; Canals, M.; Lastras, G. Geomorphic response of submarine canyons to tectonic activity: Insights from the cook strait canyon system, New Zealand. *Geosphere* **2014**, *10*, 905–929. [[CrossRef](#)]
212. Anzidei, M.; Bosman, A.; Carluccio, R.; Casalbore, D.; Caracciolo, F.D.; Esposito, A.; Nicolosi, I.; Pietrantonio, G.; Vecchio, A.; Carmisciano, C.; et al. Flooding scenarios due to land subsidence and sea-level rise: A case study for Lipari island (Italy). *Terra Nova* **2017**, *29*, 44–51. [[CrossRef](#)]
213. Chiocci, F.L.; Casalbore, D. Unexpected fast rate of morphological evolution of geologically-active continental margins during quaternary: Examples from selected areas in the Italian seas. *Mar. Pet. Geol.* **2017**, *82*, 154–162. [[CrossRef](#)]
214. Casalbore, D.; Romagnoli, C.; Bosman, A.; Anzidei, M.; Chiocci, F.L. Coastal hazard due to submarine canyons in active insular volcanoes: Examples from Lipari island (Southern Tyrrhenian sea). *J. Coast. Conserv.* **2018**, *22*, 989–999. [[CrossRef](#)]
215. Carracedo, J.C.; Troll, V.R.; Zaczek, K.; Rodríguez-González, A.; Soler, V.; Deegan, F.M. The 2011–2012 submarine eruption off El Hierro, Canary islands: New lessons in oceanic island growth and volcanic crisis management. *Earth Sci. Rev.* **2015**, *150*, 168–200. [[CrossRef](#)]
216. Casalbore, D.; Clare, M.A.; Pope, E.L.; Quartau, R.; Bosman, A.; Chiocci, F.L.; Romagnoli, C.; Santos, R. Bedforms on the submarine flanks of insular volcanoes: New insights gained from high resolution seafloor surveys. *Sedimentology* **2020**. [[CrossRef](#)]
217. Urgeles, R.; Canals, M.; Baraza, J.; Alonso, B.; Masson, D. The most recent megalandslides of the Canary islands: El Golfo debris avalanche and Canary debris flow, West El Hierro island. *J. Geophys. Res. Solid Earth* **1997**, *102*, 20305–20323. [[CrossRef](#)]
218. Romagnoli, C.; Casalbore, D.; Chiocci, F.L.; Bosman, A. Offshore evidence of large-scale lateral collapses on the eastern flank of Stromboli, Italy, due to structurally-controlled, bilateral flank instability. *Mar. Geol.* **2009**, *262*, 1–13. [[CrossRef](#)]
219. Coombs, M.L.; White, S.M.; Scholl, D.W. Massive edifice failure at Aleutian Arc volcanoes. *Earth Planet. Sci. Lett.* **2007**, *256*, 403–418. [[CrossRef](#)]
220. Casalbore, D.; Bosman, A.; Chiocci, F.L. Study of Recent Small-Scale Landslides in Geologically Active Marine Areas Through Repeated Multibeam Surveys: Examples from the Southern Italy. In *Submarine Mass Movements and Their Consequences*; Yamada, Y., Kawamura, K., Ikehara, K., Ogawa, Y., Urgeles, R., Mosher, D., Chaytor, J., Strasser, M., Eds.; Springer: Dordrecht, The Netherlands, 2012; pp. 573–582.
221. Casalbore, D.; Passeri, F.; Tommasi, P.; Verrucci, L.; Bosman, A.; Romagnoli, C.; Chiocci, F.L. Small-scale slope instability on the submarine flanks of insular volcanoes: The case-study of the Sciara del Fuoco slope (Stromboli). *Int. J. Earth Sci.* **2020**, *109*, 2643–2658. [[CrossRef](#)]
222. Maramai, A.; Graziani, L.; Tinti, S. Tsunamis in the Aeolian islands (Southern Italy): A review. *Mar. Geol.* **2005**, *215*, 11–21. [[CrossRef](#)]
223. Carey, S.; Sigurdsson, H.; Mandeville, C.; Bronto, S. Volcanic Hazards from Pyroclastic Flow Discharge into the Sea: Examples from the 1883 Eruption of Krakatau, Indonesia. In *Volcanic Hazards and Disasters in Human Antiquity*; McCoy, F.W., Heiken, G., Eds.; Geological Society of America: Boulder, CO, USA, 2000; Volume 345, pp. 1–14.
224. Chiocci, F.L.; Romagnoli, C.; Tommasi, P.; Bosman, A. The stromboli 2002 tsunamigenic submarine slide: Characteristics and possible failure mechanisms. *J. Geophys. Res.* **2008**, *113*, B10102. [[CrossRef](#)]
225. Caress, D.W.; Clague, D.A.; Paduan, J.B.; Martin, J.F.; Dreyer, B.M.; Chadwick, W.W.; Denny, A.; Kelley, D.S. Repeat bathymetric surveys at 1-metre resolution of lava flows erupted at Axial seamount in April 2011. *Nat. Geosci.* **2012**, *5*, 483–488. [[CrossRef](#)]
226. Chadwick, W.W.; Dziak, R.P.; Haxel, J.H.; Embley, R.W.; Matsumoto, H. Submarine landslide triggered by volcanic eruption recorded by in situ hydrophone. *Geology* **2012**, *40*, 51–54. [[CrossRef](#)]
227. Carey, R.; Soule, S.A.; Manga, M.; White, J.; McPhie, J.; Wysoczanski, R.; Jutzeler, M.; Tani, K.; Yoerger, D.; Fornari, D.; et al. The largest deep-ocean silicic volcanic eruption of the past century. *Sci. Adv.* **2018**, *4*, e1701121. [[CrossRef](#)] [[PubMed](#)]

-
228. Chadwick, W.W.; Rubin, K.H.; Merle, S.G.; Bobbitt, A.M.; Kwasnitschka, T.; Embley, R.W. Recent eruptions between 2012 and 2018 discovered at West Mata submarine volcano (NE Lau Basin, SW Pacific) and characterized by new ship, AUV, and ROV data. *Front. Mar. Sci.* **2018**, *6*, 495. [[CrossRef](#)]
229. Gaspar, J.L.; Queiroz, G.; Pacheco, J.M.; Ferreira, T.; Wallenstein, N.; Almeida, M.H.; Coutinho, R. Basaltic Lava Balloons Produced During the 1998–2001 Serreta Submarine Ridge Eruption (Azores). In *Explosive Subaqueous Volcanism*; White, J.D.L., Smellie, J.L., Clague, D.A., Eds.; American Geophysical Union: Washington, DC, USA, 2003; pp. 205–212.